

PATHWAYS AND MECHANISMS FOR THERMOLYSES OF METHYLATED ACENES

P.S. Virk and V.J. Vlastnik
Department of Chemical Engineering
M. I. T., Cambridge, MA 02139

KEYWORDS: Thermolysis, Reaction Paths, Kinetics, Demethylation, Hydrogen Transfer.

ABSTRACT: Thermolyses of three methylated aromatic acenes, 9,10-Dimethyl-Anthracene (910DMA), 9-Methyl-Anthracene (9MA), and 1,4-Dimethyl-Naphthalene (14DMN), were studied to mimic the thermal decomposition of methyl-substituted aromatic moieties in coal and coal liquids. Experiments were conducted at temperatures from 315-550 C, initial substrate concentrations from 0.08-2.5 mol/l, and fractional substrate conversions, X , from 0.05-0.99. The observed thermolysis kinetics ranged from $\sim 3/2$ to 2 order wrt substrate, with activation energies ~ 45 kcal/mol. At fixed $T = 370$ C and $[C]_0 \sim 0.85$ mol/l, decomposition half-lives for (910DMA, 9MA, 14DMN) were respectively (9900, 23000, 530000) s. In general, three primary pathways operated during thermolysis of these methylated acenes. For 910DMA these were: (P1) Hydrogenation, to 9,10-Dihydro-9,10-Dimethyl-Anthracene, (P2) Demethylation, to 9-Methyl-Anthracene, and (P3) Methylation, to 1,9,10-Trimethyl-Anthracene (and isomers). These pathways further operate upon the primary products themselves, forming 9,10-Dihydro-9-Methyl-Anthracene, a host of Dimethyl-Anthracenes (1,9-, 1,10-, 2,9-, and 3,9-isomers), and Anthracene, as well as 1- and 2-Methyl-Anthracenes. Observed initial selectivities to the primary hydrogenation, demethylation, and methylation products were respectively about 0.1, 0.3 and 0.1, while the selectivities to methane gas and to heavy products were respectively 0.2 and 0.2. A radical mechanism comprising 10 elementary steps was proposed for 910DMA thermolysis at low conversions, and shown to account for the experimental observations.

INTRODUCTION

Motivation. The present work on thermolysis of methylated aromatic acenes is part of a continuing study [1,2] of simple substrates that mimic the chemical moieties found in complex fossil materials of engineering interest. The 910DMA, 9MA and 14DMN substrates were chosen because their acene rings are prototypical of the aromatic ring systems found in fossil materials, while their methyl groups model the electron-donating substituents commonly pendant thereon.

Previous Work. Neither 910DMA nor 14DMN thermolyses appear to have been studied previously. The literature contains two earlier references to 9MA thermolysis [3, 4].

Outline. We first describe the experiments and present results for the concentration histories, product selectivities, and kinetics observed during 910DMA thermolysis. These results are combined with data from 9MA and 14DMN thermolyses to provide general reaction pathways for the decomposition of multiply-methylated acenes. Finally, a radical mechanism comprising 10 elementary steps is proposed for 910DMA thermolysis at low conversions, and shown to accommodate many of the experimental observations.

EXPERIMENTAL

Conditions. The upper portion of Table 1 summarizes conditions for the experiments, listing the model substrates, their structures and the ranges of temperatures, holding times and initial concentrations studied, as well as the temperatures at which light gases were analysed. Thermolyses were conducted in batch reactors, volume 0.6 ml, made from 1/4" stainless steel Swagelok parts. The reactors were charged with weighed amounts of biphenyl (internal standard) and substrate (say, 910DMA) totalling 0.30 g, sealed and placed in an isothermal, fluidized-sand bath for the appropriate holding times, after which they were quenched in ice-water, and their contents extracted into methylene chloride. Reactor contents were in the liquid phase during all experiments.

Assays. Gaseous and liquid thermolysis products were identified and analyzed by GC, augmented by GC/MS. All gas peaks were identified by injections of standards. Most liquid products were identified by injections of standards with some minor liquid products identified by determining their masses by GC/MS and relating their retention times to those of known molecules. Heavy thermolysis products, mostly dehydrogenated dimers of the substrates, were identified by GC/MS. For example, in 910DMA thermolyses, the MS of a prominent late GC peak showed a molecular ion at mass 410 and a fragment at mass 205, suggestive of a bibenzyl, dehydrogenated dimer of 910DMA. Product assay trains developed for each substrate using the preceding GC and GC/MS techniques typically identified ~ 15 reaction products. Identified products accounted for $> 90\%$ of the reacted mass at low substrate conversion, $X < 0.4$, and $> 65\%$ of the reacted mass at the highest conversions, $X > 0.8$. Experimental details are available [5].

RESULTS and DISCUSSION

Histories. Fig. 1 chronicles the concentration histories of substrate and products during thermolysis of 910DMA at $T = 370$ C and $[C]_0 = 0.82$ mol/l, using arithmetic coordinates of absolute mols J of either substrate or product present in the reactor versus reaction holding time t in seconds. Part (a), left panel, shows that the substrate 910DMA decayed monotonically, with half-life $t^* \sim 9000$ s. The major products formed, in order of initial abundance, were 9MA, methane, abbr CH_4 , various trimethyl-anthracenes, abbr TMA, dihydro-dimethyl-anthracenes, abbr DHDMA, and anthracene, abbr ANT. The main product 9MA exhibited a maximum, characteristic of an intermediate in the demethylation sequence $910DMA \rightarrow 9MA \rightarrow$

ANT. The formation of TMA and DHDMA products concurrent with 9MA shows that during 910DMA thermolysis, methylation and hydrogenation always occur in parallel with demethylation. Part (b), right panel, shows minor product histories, including those of the dimethyl-anthracene isomers, 1,9-, 1,10-, 2,9-, and 3,9-DMA, all of which arose subsequent to 9MA, the methyl-anthracene isomers, 1MA and 2MA, both of which arose subsequent to ANT, and the 9,10 dihydro- hydrogenated species, DHMA and DHA, both formed subsequent to their parent aromatic. The foregoing suggest that the minor 1,9-, 1,10-, 2,9-, and 3,9-DMA products originated by methylation of 9MA rather than the isomerization of 910 DMA substrate and also that 1MA and 2MA likely arose from methylation of ANT rather than isomerization of 9MA.

Selectivities. Fig. 2 depicts the preceding product history data as selectivity diagrams, with ordinate of product selectivity $S = \text{mols J produced/mol of substrate 910DMA decomposed}$, and abscissa of substrate fractional conversion X . Part (a), left panel, shows that the products formed at the lowest conversions were 9MA, TMA, and CH₄ with selectivities respectively $S = 0.35, 0.20$ and 0.20 , as well as DHDMA and ANT, with respective $S \sim 0.06$ and 0.03 . With increasing conversion, 9MA selectivity remained roughly constant at $S \sim 0.4$ for $X < 0.80$, while TMA and CH₄ exhibited mirror image selectivity decreases and increases, likely reflecting demethylation of the TMA; the selectivity of DHDMA decreased monotonically, to near zero at the highest conversions, while ANT selectivity increased monotonically, reflecting its position as demethylation terminus. The sum of the selectivities of all identified liquid products (circles) was ~ 0.75 over the major range of conversions, $0.2 < X < 0.8$, from which the selectivity of unidentified, mostly heavy, product formation is inferred to be ~ 0.25 .

Product Ratios. The importance of each of the observed hydrogenation, methylation, and methane formation pathways relative to the dominant demethylation pathway can be assessed from the respective primary product ratios R , namely $R[\text{DHDMA}/9\text{MA}]$, $R[\text{TMA}/9\text{MA}]$ and $R[\text{CH}_4/9\text{MA}]$. Of these, the ratio of hydrogenation to demethylation, $R[\text{DHDMA}/9\text{MA}] \rightarrow 0.4$ at the lowest conversions, $X \rightarrow 0$, and then decreased rapidly to 0.04 ± 0.02 for $X > 0.20$. This variation of $R[\text{DHDMA}/9\text{MA}]$ versus X was essentially independent of initial concentration and temperature, implying that the hydrogenation and demethylation pathways were of similar overall order wrt substrate and possessed similar activation energies. Fig. 3(a), left panel, shows that the ratio of methylation to demethylation, $R[\text{TMA}/9\text{MA}] = 0.24$ for $X > 0.20$ at all temperatures while Fig. 3(b), right panel, shows that the ratio of methane formation to demethylation, $R[\text{CH}_4/9\text{MA}] = 0.63$ for $X > 0.20$ at $T = 355$ and 370°C . The sum $R[\text{TMA}/9\text{MA}] + R[\text{CH}_4/9\text{MA}] \sim 0.87$ was close to unity, accounting for the methyl radicals implicitly associated with the demethylation pathway. It is interesting that $\sim 3/4$ of all methyl radicals formed were quenched by hydrogen abstraction, forming methane gas, while $\sim 1/4$ were trapped by addition to the 910DMA substrate, eventually appearing as TMAs.

Kinetics. Observed decomposition kinetics are illustrated in Fig. 4. Part (a), left panel, is a log-log plot of decay half-life t^* versus initial concentration $[C]_0$ at fixed temperature. The data for 910DMA substrate (circles), spanning two decades of $[C]_0$, describe a line of slope $-1/2$, which implies that the decomposition was of $3/2$ order wrt substrate. Part (b), right panel, is an Arrhenius type of semi-log plot, showing decay half-life t^* versus the reciprocal of a scaled absolute temperature $\Theta = 0.004573^\circ\text{T} (\text{C} + 273.2)$. Data for 910DMA substrate (circles), spanning two decades of t^* , define a line of slope -43 ; on these coordinates, the slope is directly the activation energy of decomposition E^* , in kcal/mol. Decay half-lives obtained for thermolyses of the other substrates, 9MA (squares) and 14DMN (triangles) are also shown in Fig. 4. Kinetics are summarized in Table 1, in the form of decay half-lives at $T = 370^\circ\text{C}$, orders wrt substrate, and Arrhenius parameters ($\log A$, E^*). The relative decomposition rates of 910DMA, 9MA, and 14DMN were roughly in the ratio $1 : \sim 1/2 : \sim 1/50$. All decompositions were of high order, between $3/2$ and 2 , wrt substrate, and exhibited activation energies ~ 45 kcal/mol.

Pathways. The concentration history, selectivity and product ratio observations detailed for 910DMA substrate were broadly echoed in thermolyses of the other two substrates, 9MA and 14DMN, as well. From these results, general decomposition pathways for multiply-methylated acenes containing, say, X total methyl substituents were deduced. Fig. 5 shows that three primary pathways operate in parallel upon the original X -Methyl Acene, namely: (P1) Hydrogenation, to the Dihydro- X -Methyl Acene, (P2) Demethylation, to the $(X-1)$ -Methyl-Acene, and (P3) Methylation, to the $(X+1)$ -Methyl-Acene. Too, the demethylated acene product is associated with formation of methane gas CH₄, and the scheme also includes formation of a heavy bibenzyl dimer of the X -Methyl Acene. Further, the primary demethylation and methylation products in the above scheme can be secondarily operated upon by a pathway triad analogous to the one from which they arose, leading respectively to the formation of $(X-2)$ - and $(X+2)$ -Methyl Acenes, and thence, recursively, to all levels of methylation from the denuded parent to the fully methylated acene nucleus. In 910DMA thermolysis the primary pathway triad is (P1) Hydrogenation, to DHDMA, (P2) Demethylation, to 9MA, and (P3) Methylation, to TMA. Continued operation of this general pathway triad upon the primary products is evidenced by the appearance, at high conversions, of DHMA, a host of DMAs (1,9-, 1,10-, 2,9-, and 3,9-isomers), ANT, and 1MA and 2MA. Pathway results for all substrates are summarized in the bottom sections of Table 2, which show, in generalized form, major product selectivities and ratios at $T = 370^\circ\text{C}$ and conversions $X = 0.05$ and 0.4 . Results for 9MA were qualitatively similar to those obtained for 910DMA, but showed a two-fold greater selectivity to the methylated product, and also roughly two-fold greater ratios of hydrogenated/demethylated and of methylated/demethylated products at low conversions. Results for 14DMN were noteworthy in that the hydrogenation pathway (P2) was essentially absent, with other product selectivities and ratios akin to those for 910DMA.

Mechanism. A possible mechanism for 910DMA thermolysis is presented in Fig. 6. This elementary step "graph" is constructed with substrate and all stable molecular products arrayed in the bottom row and unstable radical intermediates arrayed in the top row. Reaction "nodes", arrayed in the middle row, connect the individual species in the bottom and top rows with arrows indicating the initial direction of reaction (all reactions are, of course, reversible). Arrow thicknesses are set roughly proportional to elementary reaction traffic, as inferred from the observed product selectivities. Initiation reactions are denoted by solid interconnecting lines, propagation reactions by various kinds of dashed lines and termination reactions by dotted lines. The 910DMA substrate is in the middle of the bottom row, with light (propagation) products to its right and heavy (termination) products, to its left. The free-radical cycle is initiated by the bimolecular disproportionation of substrate (R1), an intermolecular hydrogen transfer reaction, to form the respectively dehydrogenated and hydrogenated radical species 910DMA* and HDMA*. Of these, the latter can either abstract hydrogen from 910DMA by (R2), to form DHDMA products, or undergo a β -scission type of radical decomposition by (R3), forming 9MA product and a methyl radical CH_3^* . The CH_3^* can either abstract H from 910DMA by (R4), to form methane product, or add to 910DMA by (R5), to form the trimethyl radical HTMA1*. The latter can then abstract H from 910DMA via (R6) to form the observed TMA product. The radical cycle is terminated by the species 910DMA* and HDMA* engaging in both pure- and cross-combinations, (R7-R9), to form various dimeric products. HDMA* radical can also terminate by disproportionation, (R10), to form 910DMA and DHDMA.

The proposed mechanism evidently accounts for most of the major products, 9MA, TMA, DHDMA, CH_4 and heavies, observed during the initial stages of 910DMA thermolysis. Each of the observed triad of primary pathways, namely, P1 hydrogenation, P2 demethylation and P3 methylation, also arise naturally as limiting cases of the elementary step graph, with P1 comprising the set [R1, R2, R7], P2 the set [R1, R3, R4, R7] and P3 the set [R1, R3, R5, R6, R8]. The stoichiometry of these sets restricts the maximum selectivity of each major product to 1/3, which is of the magnitude of the highest selectivities actually observed. The mechanism also offers some theoretical insights. It suggests that the relative kinetics of the observed hydrogenation and demethylation pathways, (P1)/(P2), are essentially controlled by the HDMA* radical, through the ratio of its H-abstraction to β -scission reactions (R2)/(R3). Further, the observed methylation to demethylation pathway ratio, (P3)/(P2), is essentially governed by competition between methyl radical reactions (R4) and (R5), in which CH_3^* either abstracts H from or adds to the 910DMA substrate.

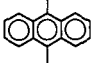
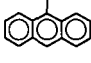
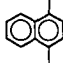
In future work it is hoped that the mechanism presented above will provide a basis for both the further quantitative modelling and numerical simulation of 910DMA thermolysis and also for the construction of new, analogous, mechanisms for 9MA and 14DMN thermolyses.

ACKNOWLEDGEMENT: This work was supported by Cabot Corporation, Boston, MA.

REFERENCES

- [1] Virk, P.S.; Vlastnik, V.J.: PREPRINTS, Div. of Petrol. Chem., ACS, 38(2), 422 (1993).
- [2] Virk, P.S.; Vlastnik, V.J.: PREPRINTS, Div. of Fuel Chem., ACS, 37(2), 947 (1992).
- [3] Pomerantz, M.; Combs Jr., G.L.; Fink, R.: J. Org. Chem., 45, 143 (1980).
- [4] Smith, C.M.; Savage, P.E.: A.I.Ch.E. J., 39, 1355 (1993).
- [5] Vlastnik, V.J.: Sc.D. Thesis, Dept. of Chem. Eng., MIT, Cambridge, MA (1993).

Table 1. Experimental Grid, Kinetics, and Major Product Selectivities and Ratios for Thermolyses of Methylated Acenes.

| Substrate Structure | | 910DMA | 9MA | 14DMN |
|-------------------------------------------------|----------|-------------------------------------------------------------------------------------|-------------------------------------------------------------------------------------|-------------------------------------------------------------------------------------|
| | |  |  |  |
| Experimental Grid | | | | |
| Temperature, T C | | 315-409 | 315-409 | 370-550 |
| Holding Time, t s | | 450-57600 | 450-57600 | 150-115200 |
| Initial Concentration, [C] ₀ , mol/l | | 0.082-2.47 | 0.082-2.06 | 0.081-2.07 |
| Gas Analyses at T C | | 335, 370 | 370 | 450 |
| Kinetics | | | | |
| Decay Half-Life, t* s at T = 370 C | | 9900 | 23000 | 530000 |
| Order wrt substrate | | 1.53 | 1.50 | 2.05 |
| Arrhenius Parameters (log A, E*) | | (10.6, 43.1) | (11.4, 46.4) | (8.5, 42.0) |
| Product Selectivities at T = 370 C | X | | | |
| Demethylated | 0.4 | 0.42 | 0.37 | 0.32 |
| Methylated | 0.4 | 0.10 | 0.22 | 0.10 |
| Hydrogenated | 0.05 | 0.06 | 0.03 | 0 |
| Heavies | 0.4 | 0.15 | 0.13 | 0.06 |
| Product Ratios at T = 370 C | X | | | |
| [Hydrogenated/Demethylated] | 0.05 | 0.21 | 0.43 | 0 |
| | 0.4 | 0.04 | 0.05 | 0 |
| [Methylated/Demethylated] | 0.05 | 0.35 | 0.69 | 0.54 |
| | 0.4 | 0.28 | 0.36 | na |

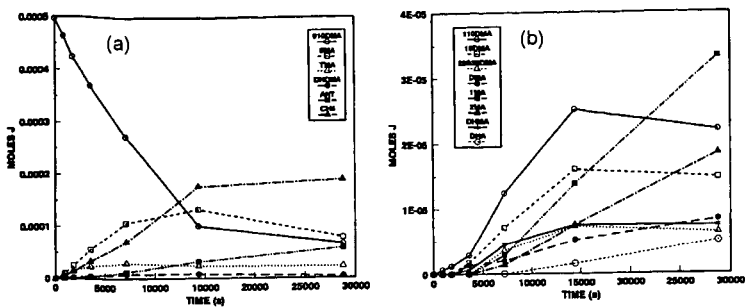


Fig. 1. Concentration Histories in 910DMA Thermolysis at $T = 370\text{ C}$ and $[910\text{DMA}]_0 = 0.82\text{ mol/l}$. (a) Major and (b) Minor Products.

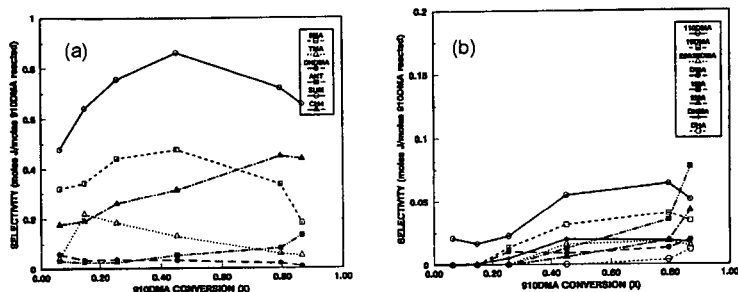


Fig. 2. Product Selectivities in 910DMA Thermolysis at $T = 370\text{ C}$ and $[910\text{DMA}]_0 = 0.82\text{ mol/l}$. (a) Major and (b) Minor Products.

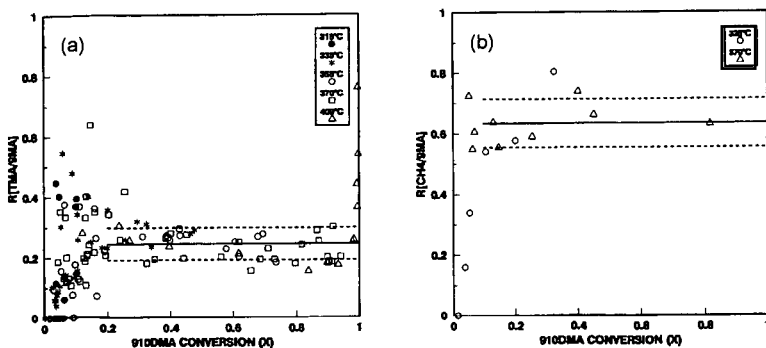


Fig. 3. Major Product Ratios in 910DMA Thermolyses at $T = 315\text{ to }409\text{ C}$ and $[910\text{DMA}]_0 = 0.82\text{ mol/l}$. (a) $R[\text{TMA}/9\text{MA}]$ and (b) $R[\text{CH}_4/9\text{MA}]$.

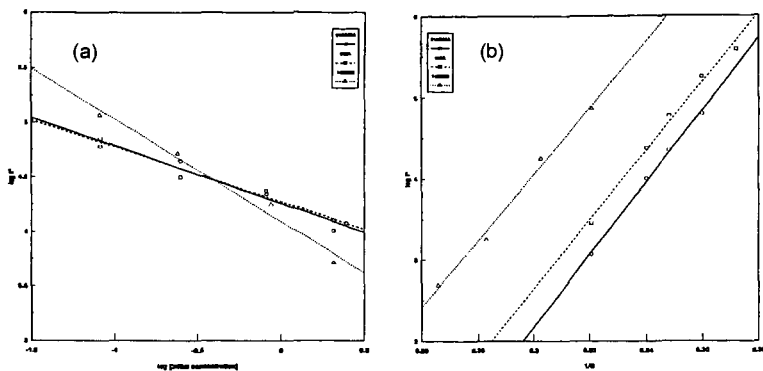


Fig. 4. Decay Half-Lives in Methylated Acene Thermolyses. (a) Effect of Initial Concentration at Fixed $T = 355^\circ\text{C}$ (910DMA), 370°C (9MA), and 450°C (14DMN), and (b) Effect of Temperature at Fixed $[C]_0 \sim 0.85 \text{ mol/l}$ (all).

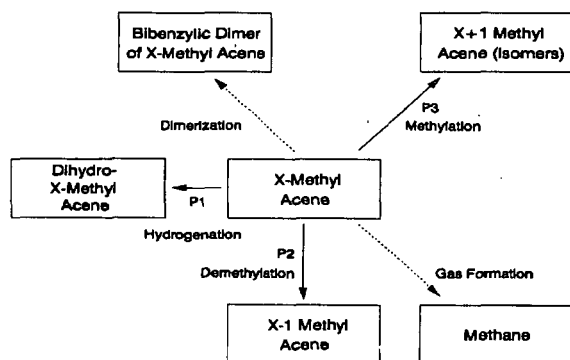


Fig. 5. General Decomposition Pathways for an X-Methyl Acene.

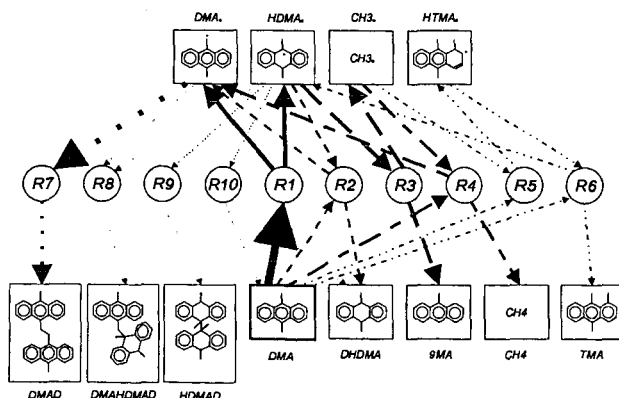


Fig. 6. Elementary Step Graph of 910DMA Thermolysis Mechanism Showing Relative Reaction Traffic at Low Substrate Conversions.

SULPHUR-CONTAINING PHENOL-FORMALDEHYDE RESINS TO MODEL THE THERMAL CHEMISTRY OF ORGANIC SULPHUR FORMS IN COALS

Khudzir Ismail, Gordon D. Love, Stuart C. Mitchell, Stephen D. Brown and Colin E. Snape

University of Strathclyde, Dept. of Pure and Applied Chemistry, Glasgow, G1 1XL, UK.

Keywords: Temperature programmed reduction, calibration, hydropyrolysis, retrogressive chemistry.

ABSTRACT

Non-melting silica immobilised substrates have previously been used to investigate pyrolysis behaviour and were shown to be ideal calibrants for temperature programmed reduction (TPR), with the SiO-C linkage stable at temperatures above 500°C. An alternative class of materials that should prove equally suitable are phenol-formaldehyde resins which enable model moieties to be incorporated into a highly cross-linked matrix. A series of sulphur containing co-resites have been prepared using phenol with, as the second component, dibenzothiophene, diphenylsulphide, phenylbenzylsulphide and thioanisole. A mole ratio of 3:1 (phenol to sulphur-containing component) was adopted to ensure that a reasonably high degree of cross-linking was achieved in the initial preparation of the resoles. The formation of the resites by curing the resoles at 200°C was monitored by solid state ¹³C NMR. A resole has also been prepared from diphenyldisulphide but due to the comparable bond strengths of the S-S and C-O linkages, the curing temperature was reduced to 120°C to avoid cleavage of the disulphide bond. As well as being used as calibrants for TPR, the resites offer considerable potential for probing the influence of catalysts in hydropyrolysis and for investigating the effect of pyrolysis conditions on the interconversion of sulphides into thiophenes.

INTRODUCTION

In order to obtain insights into the complex reactions which occur during the pyrolysis and liquefaction of solid fuels, detailed structural information about the starting material and an understanding of how the different functionalities present behave under processing conditions are required. To achieve the latter aim, model compound studies performed in both the vapour and liquid phases have been used extensively ⁽¹⁾. However, a major drawback with such studies is the fact that the radicals generated via bond homolysis are mobile and free to diffuse independently prior to further reaction. In contrast, for solids such as coals and oil shales, many of the reactive intermediates remain covalently attached to the cross-linked macromolecular framework and thus their reactivity is subject to diffusional restraints.

In order to explore the effects of restricted mobility in multipathway free-radical reactions, Buchanan and coworkers pioneered work on model compounds immobilised on silica ^(2,4). Recently, a series of silica immobilised diphenylalkanes and sulphur-containing substrates have been used at Strathclyde to study solid fuel pyrolysis phenomena. In addition, the sulphur-containing substrates have been used as calibrants for temperature programmed reduction (TPR) ^(5,6); a technique based on the principle that different organic sulphur forms present in solid fuels have different characteristic reduction temperatures at which hydrogen sulphide (H₂S) evolves. Previously, the technique had met with only limited success, primarily because only

labile non-thiophenic forms were observed. Poor overall sulphur balances resulted, with virtually all the thiophenic sulphur remaining in the char due to the low pressures and the low boiling reducing agents used (7-10). Further, little account has been taken of the reduction of pyrite to pyrrhotite and retrogressive reactions, particularly the conversion of sulphides into thiophenes. These drawbacks have been overcome by the use of a well-swept fixed-bed reactor operating at relatively high hydrogen pressures (up to 150 bar) (11,12). Typically, over 70% of the organic sulphur is reduced to H_2S with the remainder being released in the tars. The use of effective catalysts, such as sulphided molybdenum can further improve the extent of desulphurisation (13).

In contrast to the reflux-type reactors used in low (atmospheric) pressure TPR studies (7-10) where liquids have been used for calibration, solids which do not soften prior to the onset of thermal decomposition are essential due to the nature of the well-swept high pressure reactor (5,6). In this respect, non-melting silica immobilised substrates are ideal, as demonstrated by immobilised benzene where the Si-O-C linkage was found to be stable to ca 500°C, even in reducing atmospheres (14). Immobilised samples of dibenzothiophene, diphenylsulphide, benzylphenylsulphide and thioanisole were subsequently prepared and used as calibrants (5,6) for both the well-swept high pressure and a reflux-type low pressure TPR reactor. Further, the substrates were found to be suitable for probing coal and oil shale pyrolysis mechanisms at temperatures in the range 400-600°C, generally used to maximise tar yields in both fluidised and well-swept bed reactors.

An alternative class of materials that should prove equally suitable are phenol-formaldehyde resins which offer the option of incorporating a wide variety of sulphur-containing moieties. A series of co-resites have been prepared using phenol together with a series of sulphur-containing precursors; 2-hydroxydibenzothiophene, *p*-hydroxydiphenylsulphide, 4-hydroxyphenylbenzylsulphide and 4-hydroxythioanisole, the same precursors used previously for the preparation of silica-immobilised substrates (5,6). A resole has also been prepared using dihydroxydiphenyldisulphide (DHPDS). This paper details the monitoring of the curing treatment by ^{13}C solid state NMR and the desulphurisation behaviour, of the formed resites, by high pressure temperature programmed reduction (TPR).

EXPERIMENTAL

Synthesis Thioanisole was the only commercially-available precursor used. 2-Hydroxydibenzothiophene was prepared via the base hydrolysis of the corresponding bromo derivative (15). Benzene sulphinic acid was reacted with phenol using a modification of Hinsberg's method (16) to prepare 4-hydroxydiphenylsulphide. 4-hydroxyphenylbenzylsulphide was prepared by reacting 4-hydroxythiophenol with benzylbromide (17). 4-hydroxythiophenol was oxidised with dimethyldithiobis(thioformate) to yield 4,4'-dihydroxydiphenyldisulphide (18).

The co-resites were prepared using the procedure described by Bar and Aizenshtat (19) with a phenol to formaldehyde mole ratio of 1:2.5. The mole ratio of phenol to the sulphur-containing component was 3:1 to ensure that a reasonably high degree of crosslinking was achieved in the initial resoles and ca 6 weight % sulphur was present in the final cured resites. Sodium hydroxide was used as catalyst in the condensation reaction with mole ratio of 0.1 with respect to phenol. The resites were cured in an oven purged with nitrogen gas at a temperature of 200°C. The resin containing DHPDS was prepared without addition of phenol and was partially cured at the much lower temperature of 130°C to avoid cleaving the disulphide bonds.

¹³C-NMR Analysis Solid state ¹³C NMR was used to follow the removal of the ether/alcohol functional groups which occurred during curing. Cross polarisation/magic-angle spinning (CP/MAS) spectra were obtained using a Bruker MSL100 instrument operating at 25MHz for carbon. A contact time of 1 ms and a recycle delay of 1.5s were employed.

High pressure TPR Details on the high pressure system are described elsewhere^(5,6,12,13). As previously, a hydrogen pressure of 150 bar was used with a heating rate of 5°C/min over the range 100-600°C. Typically, between 0.2 and 0.3 g of the resite (particle size range of ca 0.1-1.0 mm) was mixed with 2-3 g sand. Hydrogen sulphide and other volatiles evolved were detected on-line using a quadrupole mass spectrometer (VG Sensorlab, 0-300 a.m.u.).

RESULTS AND DISCUSSION

Characterisation of the co-resites The elemental compositions of the cured co-resites and the disulphide resole, together with their chloroform solubilities are listed in Table 1. These results indicate that the desired level of sulphur incorporation (ca 6% w/w) has been achieved and that the resites are macromolecular in character with chloroform solubilities below 1% w/w. The DHDPPDS resole obviously contains a much higher sulphur content than the resites because of the disulphide linkage and the fact that phenol was not employed in the preparation.

Figure 1 shows the CP/MAS ¹³C NMR spectra for the partially-cured (130°C) phenylbenzylsulphide and dibenzothiophene co-resites and Figure 2 compares the spectra for the partially cured dibenzothiophene resole and the corresponding resite cured at 200°C. The spectra of all four fully cured co-resites are shown in Figure 3. Table 2 summarises the assignments for the peaks observed. In the initial resoles, the peaks at ca 60 ppm and 73 ppm attributable to methylol carbon directly attached to the ortho or para position of the phenol ring and dimethylene ether carbons, respectively, dominate over the methylene bridge carbon peaks. In addition, the resoles display another intense C-O peak at ca 93 ppm due to hemiacetal carbons (OCH₂O). For the resites cured at 200°C, the spectra only contain aliphatic carbon peaks centred at 35 and 18 ppm with no major discernible peaks at 70 ppm from ether linkages.

Figure 1 indicates that the spectra of the partially-cured resites still contain major aliphatic C-O peaks which necessitated the use of a significantly higher curing temperature to eliminate all of the ether linkages. The peak at 18 ppm observed in all the spectra of the co-resites in Figure 3 is attributable to arylmethyl and, for dibenzothiophene and diphenylsulphide, its intensity is approximately one-quarter of that for the methylene peak at 35 ppm. The intensity of the 18 ppm peak in the case of the thioanisole resite is somewhat greater due to the contribution from S-CH₃.

High pressure TPR Figures 4-8 show the high pressure TPR evolution profiles of H₂S (*m/z*=34), and, where appropriate, CH₃SH (*m/z*=48), benzene (*m/z*=78), toluene (*m/z*=91) and methane (*m/z*=16), obtained for the four co-resites investigated. Figure 5 also shows the H₂S evolution profile for the DHDPPDS resole. In addition, the desulphurisation behaviour of the dibenzothiophene co-resite was also investigated with a sulphided molybdenum catalyst (nominal loading of 0.4% w/w Mo)^(13,14); the H₂S evolution profile is shown in Figure 4.

For dibenzothiophene (Figure 4), the H₂S profile is remarkably similar to that for the corresponding immobilised substrate with the temperature of maximum evolution (*T*_{MAX}) being close to 500°C⁽⁶⁾. The use of the sulphided Mo catalyst does not significantly affect the *T*_{MAX}

although the H_2S profile is surprisingly sharper. The continuation of the H_2S evolution profiles above 500°C in both cases suggests that some condensation might be occurring to form larger thiophenic structures. The sulphur balance for the dibenzothiophene resite without catalyst, indicated that virtually 100% desulphurisation was achieved with *ca* 50% of the sulphur being released as H_2S with the remainder being in the tar collected.

The primary scission of the C-S bonds in the diphenylsulphide co-resite occurs at 330°C (Figure 5), similar to the characteristic reduction temperature found for the immobilised substrate ⁽⁶⁾. The further release of H_2S at temperatures up to 600°C indicates that much of the sulphidic sulphur has been converted into complex thiophenes. The initial reduction is accompanied by the evolution of CH_3SH and the onset of toluene evolution (Figure 5) possibly via reactions with the methylene bridges. It is interesting to note that no benzene evolves below 400°C suggesting that the non-hydroxy substituted ring in the diphenylsulphide moieties may have been cross-linked by the curing process. The partially cured resole of DHDPDS gave a characteristic H_2S T_{MAX} below 300°C (Figure 5) which is similar to that found previously for cysteine ⁽⁶⁾. However, the occurrence of secondary reactions leading to the formation of sulphides and complex thiophenes was indicated by over 70% of the H_2S evolving above 320°C .

For the phenylbenzylsulphide co-resite, initial H_2S evolution occurs at *ca* 280°C (Figure 6) from the primary scission of the C-S bond. The extent of secondary chemistry is again considerably greater than found with the corresponding immobilised substrate ⁽⁶⁾. A significant amount of CH_3SH also evolves at 280°C from the C-S scission, together with some methane and toluene (Figure 6). As with diphenylsulphide no benzene was observed at low temperature presumably because it is still bound via the methylene linkages to the remainder of the resite. Figure 7 indicates that, like its phenylbenzylsulphide counterpart, the thioanisole co-resite displays complex behaviour with the bulk of the H_2S evolving after the primary reduction of the C-S bond at *ca* 300°C . The initial H_2S release is accompanied by a considerable proportion of the sulphur evolving as methyl mercaptan.

General discussion Characteristic H_2S T_{MAX} s for the primary C-S bond scissions for the co-resites were very similar to their immobilised counterparts ⁽⁶⁾. However, the nature and extent of secondary reactions clearly differ in each case with the co-resites generally displaying a much greater extent of retrogressive chemistry. This may be due to the much larger particle size used (0.1-1 mm, cf. <0.05 mm) and possibly the generation of many more diverse radical species during pyrolysis. The co-resites are, by nature, much more convenient to use than the immobilised substrates and the focus of future research will be to investigate the effects of dispersed catalysts in vehicle-solvent liquefaction, hydrolypyrolysis and batchwise hydrogenation.

ACKNOWLEDGEMENTS

The authors thank the Science & Engineering Research Council for financial support (Grant No. GR/J1/08997).

REFERENCES

1. M.L. Poutsma, *Energy & Fuels*, 1990, **4**(2), 113 and references therein.
2. A.C. Buchanan III and C.A. Biggs, *J. Org. Chem.*, 1989, **54**, 517.
3. A.C. Buchanan III, P.F. Britt and M.L. Poutsma, *Prepr. Am. Chem. Soc. Div. Fuel Chem.*, 1990, **35**(1), 217.

4. P.F. Britt and A.C. Buchanan III, *J. Org. Chem.*, 1991, **56**, 6132.
5. S.C. Mitchell, C.J. Lafferty, R. Garcia, K. Ismail, C.E. Snape, A.C. Buchanan III, P.F. Britt and E. Klavetter, *Prepr. Amer. Chem. Soc. Div. Fuel Chem.*, 1992, **37(4)**, 1691.
6. K. Ismail, R. Garcia, S.C. Mitchell, C.E. Snape, A.C. Buchanan III, P.F. Britt, D. Franco and J. Yperman, *Proc. 1993 Int. Conf. on Coal Science*, Banff, September 1993.
7. A. Attar in *"Analytical Methods for Coal and Coal Products"*, Vol III, Academic, 1979, Ch.56 and DOE/PC/30145T1 Technical Report.
8. B.B. Majchrowicz, J. Yperman, G. Reggers, J.M. Gelan, H.J. Martens, J. Mullens and L.C. van Poucke, *Fuel Process. Technol.*, 1987, **15**, 363.
9. B.B. Majchrowicz, J. Yperman, H.J. Martens, J.M. Gelan, S. Wallace, C.J. Jones, M. Baxby, N. Taylor and K.D. Bartle, *Fuel Process. Technol.*, 1990, **24**, 195.
10. B.T. Dunstan and L.V. Walker, *Final Report to Australian Nat. Energy Res. Dev. and Dem. Council* (1988).
11. C.J. Lafferty, S.C. Mitchell, R. Garcia and C.E. Snape, *Fuel*, 1993, **72**, 367.
12. S.C. Mitchell, C.E. Snape, R. Garcia, K. Ismail and K.D. Bartle, *Fuel*, accepted. Paper presented at Conference on "Coal and the Environment", Orlando, May, 1993.
13. R. Garcia, S.R. Moineio, C.J. Lafferty and C.E. Snape, *Energy & Fuels*, 1991, **5**, 582.
14. S.C. Mitchell, C.J. Lafferty, R. Garcia, K. Ismail, C.E. Snape, A.C. Buchanan III, P.F. Britt and E. Klavetter, *Energy & Fuels*, 1993, **7**, 331.
15. N.M. Cullinane, C.G. Davies and G.I. Davies, *J. Chem. Soc.*, 1936, 1435.
16. G.E. Hilbert and T.B. Johnson, *J. Am. Chem. Soc.*, 1929, **51**, 1526.
17. E. Miller and R.R. Read, *J. Am. Chem. Soc.*, 1933, **55**, 1224.
18. E.I. Stout, B.S. Shasha and W.M. Doane, *J. Org. Chem.*, 1974, **39(4)**, 562.
19. H. Bar and Z. Aizenshtat, *J. Anal. Appl. Pyrolysis*, 1991, 265.

Table 1 Elemental compositions and chloroform solubilities of the resites and the disulphide resole

| Co-Resites/Resole | %C | %H | %S | % Solubility |
|----------------------|------|-----|------|--------------|
| Dibenzothiophene | 72.3 | 4.2 | 5.4 | < 1% |
| Diphenylsulphide | 72.4 | 4.9 | 5.2 | < 1% |
| Phenylbenzylsulphide | 72.7 | 5.0 | 5.5 | < 1% |
| Thioanisole | 69.3 | 5.1 | 6.2 | < 1% |
| Diphenyldisulphide | 54.0 | 4.4 | 19.5 | n.d |

n.d = not determined

Table 2 ¹³C NMR peak assignments the resoles and resites

| Chemical Shifts (ppm) | Functional Groups Assignment |
|-----------------------|-------------------------------------------------------------------------------------------|
| 18 | Arylmethyl, ortho position relative to the OH group |
| 30, 35 and 40 | 2,2', 2,4 and 4,4'-methylene carbon, respectively |
| 58-65 | Methylol carbon, ortho or para position relative to the phenol ring, ArCH ₂ OH |
| 68-73 | Dimethylene ether linkages; Ar-CH ₂ -O-CH ₂ - |
| 95 | Hemiacetals, OCH ₂ O |
| 110-135 | Phenolic ring carbons other than C-OH |
| 152, 160 | Phenolic, C-OH; C-O, aromatic ethers |

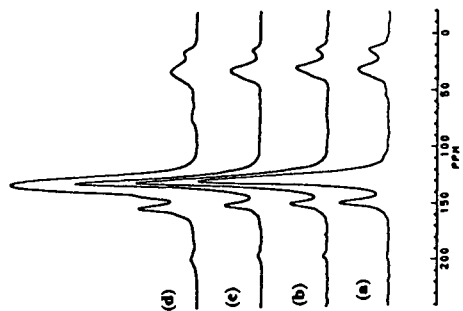
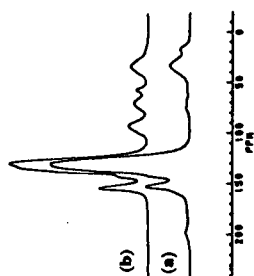
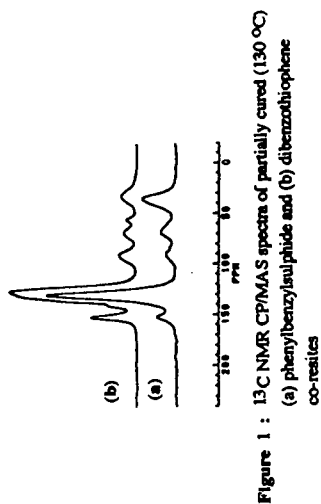


Figure 3 : ^{13}C NMR CPMAS spectra of fully cured (200 °C)
(a) thioanisole, (b) diphenylsulfide,
(c) phenylbenzylsulfide, (d) dibenzothiophene
co-resins

Figure 2 : ^{13}C NMR CPMAS spectra of (a) fully cured (200 °C)
and (b) partially cured (130 °C) dibenzothiophene co-resin

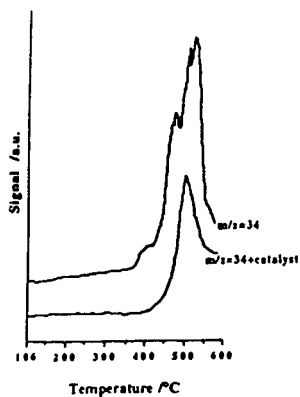


Figure 4: Hydrogen sulphide ($m/z=34$) evolution profiles for dibenzothiophene co-resite with and without catalyst

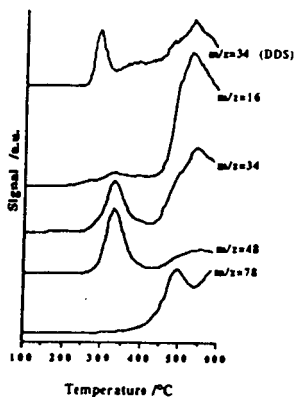


Figure 5: Evolution profiles for diphenylsulphide ($m/z=16, 34, 48$ and 78) and $m/z=34$ for diphenyldisulphide (DDS)

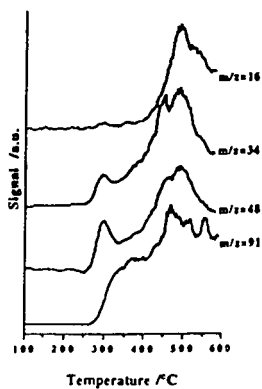


Figure 6: Evolution profiles for phenylbenzylsulphide ($m/z=16, 34, 48$ and 91)

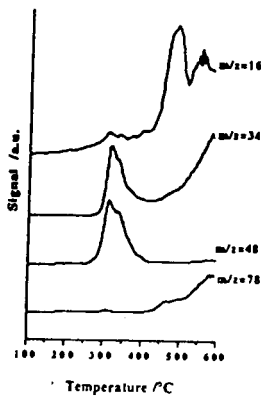


Figure 7: Evolution profiles for thioanisole ($m/z=16, 34, 48$ and 78)

INVESTIGATION OF PHYSICAL CONTROL MECHANISMS IN THE THERMAL DECOMPOSITION OF COAL BY MEANS OF ON-LINE MASS SPECTROMETRIC TECHNIQUES

Xiansheng Nie, Kui Lui, Waleed Maswadeh, Ashish Tripathi and Henk L.C. Meuzelaar

Center for Micro Analysis & Reaction Chemistry
University of Utah, Salt Lake City, UT 84112

KEYWORDS: novel TG/MS techniques; coal devolatilization mechanisms; heat and mass transport resistance

INTRODUCTION

During the past decade marked progress has been made with regard to our understanding of the chemical processes occurring during the thermal degradation ("devolatilization", "desorption + pyrolysis") of coal and several advanced mechanistic models offering a qualitative and quantitative description of these processes, e.g., FG-DVC [1] and CPD [2] models, are now available. By contrast, there appears to be a comparative lack of progress in the description and understanding of the physical processes involved. It is becoming increasingly clear that the frequent lack of interlaboratory reproducibility almost invariably originates within the physical parameters of the experiment. Although heating rate, particle size and reactor pressure have long been recognized as the dominant physical parameters influencing the rates and product yields of coal devolatilization processes [3,4], current models pay little or no attention to heat and mass transport limitations. In fact, particle size is not an input parameter in these models. Furthermore, although most industrial scale coal devolatilization processes occur at near ambient pressures, current renewed interest in high pressure coal conversion processes would seem to dictate a more detailed look at the effects of pressure.

The objective of the research reported here is to exploit the capabilities of two novel experimental techniques, based on the on-line coupling of microscale, TG-type reactors to mass spectrometry and combined gas chromatography/mass spectrometry systems. The TG/GC/MS techniques has high pressure TG capabilities [5] and will be described separately at this meeting [6]. The direct TG/MS instrument is characterized by a heated, all quartz interface and will be discussed here. The complementary nature of both systems enables us to investigate the nature and extent of physical control mechanisms over a broad range of experimental conditions.

EXPERIMENTAL

Materials - Two different particle sizes (-100 mesh and +65 -20 mesh) of all 8 ANL-PCSP coal samples (Beulah Zap, Wyodak, Illinois #6, Blind Canyon, Lewiston-Stockton, Pittsburgh #8, Upper Freeport and Pocahontas) and of a Blind Canyon DECS 6 sample were used. Only Beulah Zap and Blind Canyon DECS 6 were analyzed by high pressure TG/GC/MS. All sample ampoules were opened just before the experiment and stored under nitrogen at -26 C for max. 2 weeks.

Methods - The TG/MS system shown in Figure 1, consisting of a Perkin-Elmer TFS-2 microbalance (sensitivity 0.1 μ g, accuracy 0.1%) and a Perkin Elmer 7 series high temperature furnace was operated at heating rates between 1 and 75 K/min up to temperatures of 750 C. An Extrel EL 1000 quadrupole mass filter operating at 12 eV electron energy and a Teknivent Vector 2.2 interface combined with a PC based data system operating at scanning rates of 2.5 spectra/scan covering the 10-600 amu range.

Five to fifty mg aliquots of samples of coal were loaded into a regular platinum or specially-made "deep" gold crucible (Figure 1), and placed in the TG furnace where pyrolysis was performed in helium at atmospheric pressure. A 100 ml/min flow of helium was introduced through the top (95%) and bottom (15%) of the TG furnace. Between TG and mass spectrometer a special interface similar to an arrangement first described by Emminger and Kaisersberger [7], and consisting of concentric outer (15 mm i.d.) and inner (3 mm i.d.) quartz tubes reduces the pressure and transfers the vapor products. A countercurrent helium flow acts to direct the evolved gas and descending flows towards 80 μ m dia orifices on the upper tips of the quartz tubes. All of the sample vapors are drawn through the outer orifice and about 5% of sample vapor is drawn through the inner orifice into the MS ion source region (10^{-6} torr). The short distances between sample holder and vapor sampling inlet (< 2 cm) and between inlet and MS ion source (< 15 cm) ensure vapor product response times <2 seconds, which minimizes secondary reactions. High pressure TG experiments were performed in a TG/GC/MS system consisting of a CAHN TG-151 high pressure TG, a capillary pressure reduction line, an automated vapor sampling inlet [8], a short column transfer line GC and a HP 5871 mass selective detector (MSD). A detailed description of the system is given elsewhere [5,6].

RESULTS AND DISCUSSION

Typical examples of the type of data produced by the TG/MS system are shown in Figure 2. Note how the total ion current profile clearly matches the DTG curve, due to the special direct interface which causes little or no condensation losses. In fact, the quartz nozzle directly below the crucible (see Figure 1) remains remarkably clean even when using relatively large (e.g., 40 mg) coal samples. It should be noted that the selected ion profiles at m/z 108, 122, 110 and 142 are prominent mass signals believed to represent primarily cresols, C2 phenols, dihydroxybenzenes and methylnaphthalenes, respectively. Note that the alkylphenol profiles virtually overlap, confirming their closely similar chemical nature and origin, whereas the dihydroxybenzenes (known to consist primarily of the *ortho*-form) start evolving at a somewhat lower temperature. Finally, the methylnaphthalenes profile at m/z 142 reveals a marked contribution from low MW, bitumen-like components evolving at lower temperatures. Detailed analyses and discussions of time-resolved pyrolysis MS and TG/MS profiles from various ANL-PCSP coals can be found in earlier publications [9,10].

Effects of Pressure - DTG profiles from Beulah Zap lignite (selected because of its high moisture content), obtained at 3 different pressures are shown in Figure 3 and reveal a marked shift (approx. 100 K) in the T_{max} of the moisture loss peaks, whereas the T_{max} of the relatively small volatile matter loss peaks, known to represent primarily pyrolytic bond scission phenomena [9,10], does not shift noticeably between ambient pressure and 900 psi. This is in obvious agreement with present insight into the underlying phenomena. Moisture desorption, primarily a transport process, is sensitive to pressure changes affecting transport parameters such as viscosity and diffusivity, whereas the primarily unimolecular (first order) decomposition reactions should be more or less insensitive to pressure as long as the reactions are under chemical control, i.e., relatively free of transport limitations. The bitumen desorption component of the methylnaphthalenes signal also shifts approx. 100 K towards higher temperatures at 900 psi (not shown here). However, it would be erroneous to conclude that transfer resistances do not play a measurable role during the pyrolysis step of TG experiments at higher pressures. As shown in Figure 4, a small but definite increase in char yield (66% vs 62%) is found at 900 psi. Char formation reactions in coal obviously involve two or more reactants, and thus cannot be regarded as first order.

Effects of Heating Rate - Figure 5 demonstrates the effect of heating rate on transport resistance in Pittsburgh #8 coal. The pseudo-Arrhenius plot shown in Figure 5 is produced simply by dividing the observed evolution rates of the cresol (m/z 108) ion signal by the corresponding percent of unreacted material (assuming 100% conversion of the m/z 108 precursor moieties). The resulting "rate at constant driving force" is then plotted in the well-known natural logarithm vs. inverse temperature format without attempting to extract any Arrhenius parameters. The resulting plot provides a sensitive test for the presence of transport control. This can be understood when assuming that in an ideal instrumental set-up with "zero" response time and under experimental conditions free of transport resistances the relationship between temperature and normalized reaction rate should be independent of heating rate for first order reactions. Between 9 and 15 K/min a relatively minor shift is observed, whereas between 15 and 25 K/min, a marked shift towards higher temperatures and lower (normalized) rates signals the rapidly increasing effect of transport control. At 25 K/min, also a clear increase in char yield is observed, especially when using larger samples (with regard to particle diameter and/or bed size). This is illustrated in Figure 6 for TG weight loss profiles of Illinois #6 coal samples. However, up to 9 K/min heat and mass transport resistances appear to be minor, even when using larger coal particles (+65, -20 mesh).

Finally, a highly sensitive probe of heat and mass transport resistances can be designed when using some of the most reactive tar components, namely the *ortho*-dihydroxybenzene signals at m/z 110, as markers for secondary tar reactions. In order to compensate for variations in sample size and experimental conditions, the abundance of the signal at m/z 110 is measured against the abundance of the cresol signal at m/z 108, thus effectively using the more stable cresols as an internal standard. A similar dihydroxyaromatic/monohydroxyaromatic ratio as a measure of tar stability has been proposed by McMillen et al. [11]. Although it might have been preferable to use even more stable tar components such as the methylnaphthalenes as internal standards, the substantial contribution of bitumen-like compounds to the methylnaphthalene signals at m/z 142 (see Figure 2) poses a problem. Since secondary tar reactions tend to increase with temperature and T_{max} values increase at higher heating rates more secondary reactions are observed, as shown in Figure 7, which also illustrates the rapidly decreasing abundance of dihydroxybenzenes with increasing coal rank. This well known fact [12] may well limit the applicability of the m/z 110/108 ratio measurements to high volatile bituminous and lower rank coals. Figure 8 shows the combined effects of heating rate, particle size and bed depth on the m/z 110/108 ratio. At first approximation, the effects of each of these three parameters appear to be additive.

Particle and Bed Size Effects - More experiments need to be done at different bed depths since the only two depths (0.5 mm vs. 12.5 mm) investigated at this point represent rather extreme cases. It should be noted here that Figure 8 includes two control experiments. In order to eliminate the possibility that the difference in m/z 110/108 ratio's between the -100 mesh and +65 (-20) mesh samples could be due to chemical heterogeneities, a small aliquot of the 65 mesh coal sample was further ground to -100 mesh and found to exhibit the m/z 110/108 ratio typical of -100 mesh samples. Also, since the "deep" crucible required a larger amount of sample (40 mg) than the regular crucible (10 mg), a single run of a 40 mg sample was performed in the regular crucible (increasing the bed depth approximately 4-fold) and found to produce an m/z 110/108 ratio close to that of the regular 10 mg sample. In other words, bed depth, rather than total sample weight, appears to be the controlling factor. Closer examination of Figure 6 shows that mesh size and bed depth also do have a marked effect on char yield. These observations are echoed by the m/z 110 (dihydroxybenzene) evolution profiles in Figure 9, demonstrating the expected reduction in absolute yield as heat and mass transport resistances increase. All observations indicate that the dihydroxybenzene moieties play a significant role in the increase in char formation under transport controlled conditions. Dihydroxybenzenes are known to be prone to secondary reactions [11]. Nonetheless, all tar components appear to be involved to a varying degree with total tar yields decreasing by almost 50% when heating a 40 mg, +65 mesh sample of Illinois #6 coal at 25 K/min in a deep crucible (as compared to a 10 mg, -100 mesh sample at ≤ 10 K/min).

CONCLUSIONS

- Marked transport resistance effects on the evolution rates, yields and temperatures of key coal devolatilization products (moisture, bitumen, pyrolytic tar components) are observable under commonly used thermogravimetry conditions.
- Elevating reactor pressures to 900 psi increases the moisture as well as "bitumen" desorption Tmax values by approximately 100 K without causing a readily measurable shift in the bulk pyrolysis Tmax. However, at 900 psi, a small but consistent increase (3-5%) is seen in the amount of char formed.
- Char yield increases up to 10% are observed in ambient pressure TG experiments at higher heating rates, larger particle sizes and greater bed depth. Strong indications of increased physical control over cresol and dihydroxybenzene evolution rates are observed at heating rates above 10 K/min, particle sizes above 100 mesh and bed depths above 1 mm.
- The m/z 110/108 (primarily dihydroxybenzene/cresol) ratio is a highly sensitive indicator of increased heat and mass transport resistances as a function of heating rate, particle size and bed depth. Effects of particle size variation and bed depth appear to be additive.

ACKNOWLEDGEMENTS

This work was sponsored by the Advanced Combustion Engineering Research Center (funds for this Center are received from the National Science Foundation, the State of Utah, 23 industrial participants and the U.S. Department of Energy) and by the Consortium for Fossil Fuel Liquefaction Science (DOE grant no. UKRF-4-23576-90-10).

REFERENCES

1. Serio, M.A., Hamblen, D.G., Markham, J.R., Solomon, P.R., *Energy & Fuels*, 1987, 1, 138-152.
2. Fletcher, T.H., Kerstein, A.R., Pugmire, R.J., Solum, M.S., Grant, D.M., *Energy & Fuels*, 1992, 6, 414-431.
3. Howard, J.B., Peters, W.A., Serio, M.A. EPRI Report AP1803, EPRI, Palo Alto, CA, 1981.
4. Van Heek, K.H., Juntgen, H., *Prepr. Pap. Am. Chem. Soc., Div. Fuel Chem.*, 1984, 29,2, 2-11.
5. Nie, X.; McClennen, W.H.; Liu, K.; Meuzelaar, H.L.C. *Prepr. Pap. Am. Chem. Soc., Div. Fuel Chem.*, 1993, 38(4), 1147-1154.
6. Kui, L., Jakab, E., Meuzelaar, H.L.C., *Prepr. Pap. Am. Chem., Div. Fuel Chem.*, 1994, in press.
7. Emminger, W.D., Kaisersberger, E., *J. Thermal Anal.*, 1979, 17, 197-212.
8. Arnold, N.S., McClennen, W.H., Meuzelaar, H.L.C., *Anal. Chem.*, 1991, 63, 289-304.
9. Yun, Y., Meuzelaar, H.L.C., Simmleit, N., Schulten, H.-R., *Energy & Fuels*, 1991, 5, 22-29.
10. Simmleit, N., Schulten, H.-R., Yun, Y., Meuzelaar, H.L.C., in "Advances in Coal Spectroscopy", Plenum Press, New York, 1992, 295-338.
11. McMillen, D.F., Malholtra, R., Chang, S., Nigenda, S.E., St. John, G., EPRI Report AP-4253-SR, EPRI, Palo Alto, CA, 1985.
12. Meuzelaar, H.L.C., Harper, A.M., Given, P.H., *Proc. 5th ROMOCO Symp.* 1982, 118, 192-202.

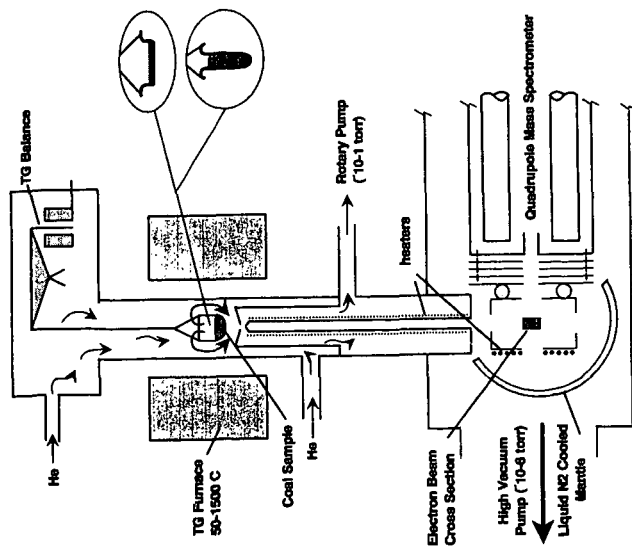


Figure 1. TG/MS system configuration. Note special flow arrangements and close proximity of crucible to concentric, heated quartz nozzles.

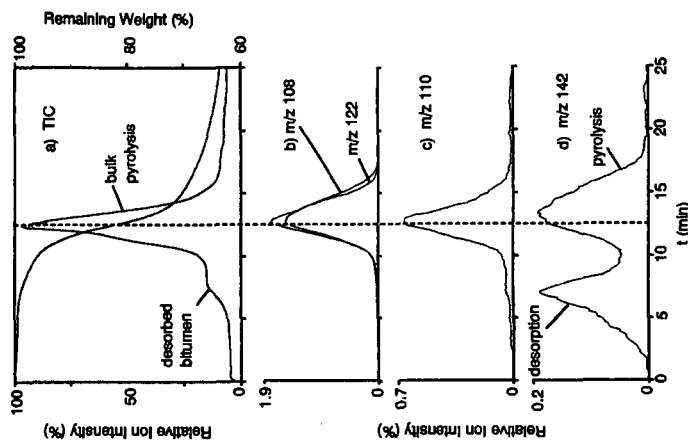


Figure 2. Example of time- and temperature-resolved TG and MS profiles from Pittsburgh #8 coal, as described in text.

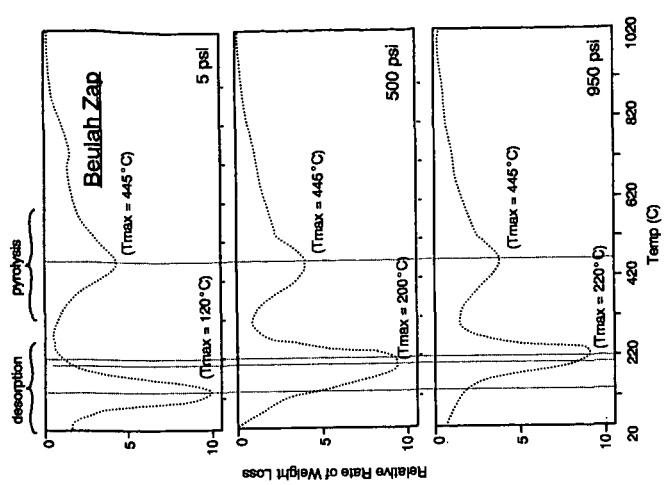


Figure 3. Comparison of DTG profiles of Beulah Zap lignite showing effect of pressure on moisture desorption Tmax.

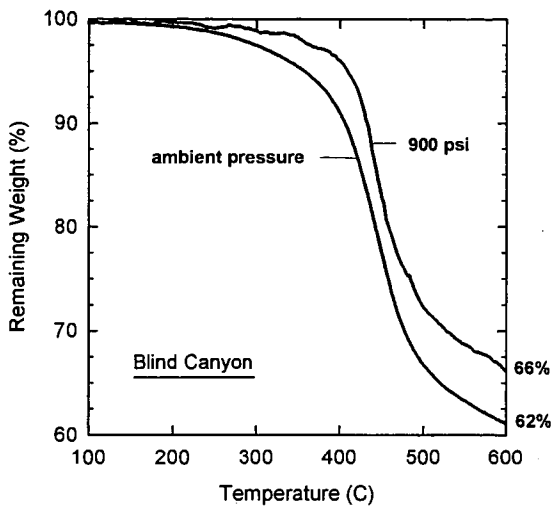


Figure 4. Effect of pressure on TG weight loss profiles for Blind Canyon Coal showing increased char residue at 600 C.

Figure 5. Pseudo-Arrhenius plot demonstrating effect of heating rate on apparent tar evolution rates (represented by cresols at m/z 108).

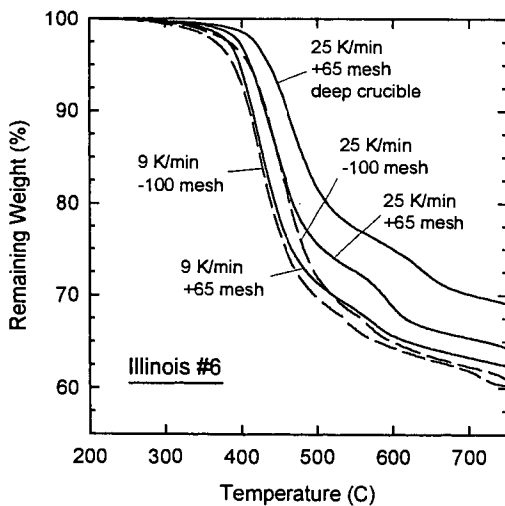
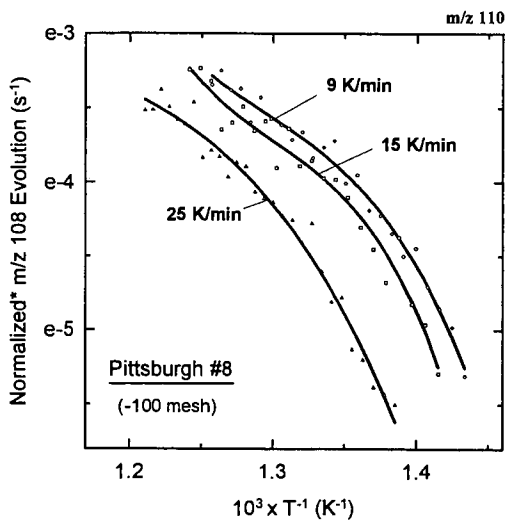


Figure 6. Effect of heating rate, particle size and bed depth on TG weight loss profiles for Illinois #6 coal (see text).

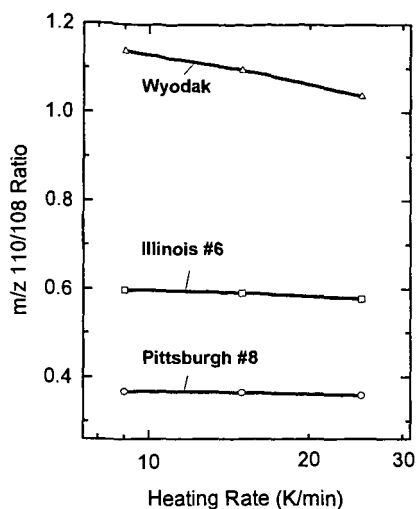


Figure 7. Effect of heating rate and coal rank on dihydroxy-benzene/cresol (m/z 110/108) ratios (see text).

Figure 8. Effect of heating rate, particle size and bed depths on m/z 110/108 ratios for Illinois #6 coal. Note m/z 110/108 ratios of 2 control samples at 25 K/min, as discussed in text.
* = +65 mesh sample reground to -100 mesh.

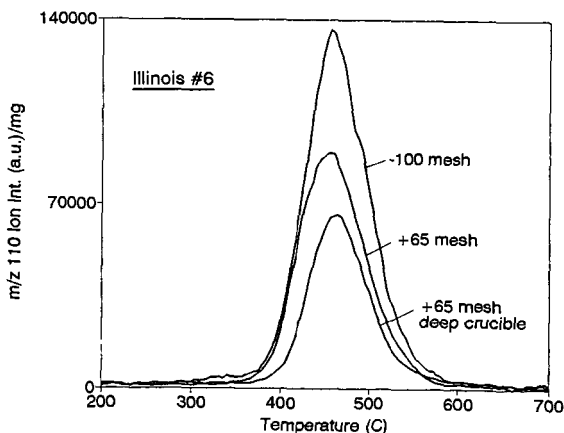
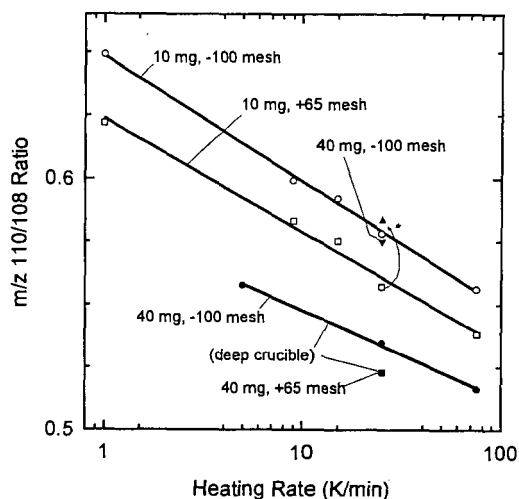


Figure 9. Effect of particle size and bed depth on dihydroxybenzene yields (corrected for sample weight) from Illinois #6 coal at 25 K/min. Note marked decrease at larger particle size and bed depth. Estimated variability between duplicate runs $\pm 5\%$ (1 day) and $\pm 10\%$ (1 week).

HIGH TEMPERATURE DEACTIVATION OF COAL CHARs

T. J. Beeley, J. R. Gibbins, R. Hurt*, C. K. Man, K. J. Pendlebury
& J. Williamson*

Department of Mechanical Engineering,

*Department of Materials, Imperial College, London SW7 2BX

*Sandia National Laboratory, Livermore, CA 94551-0969

Keywords: coal char combustion, reactivity

INTRODUCTION

High levels of char burnout, typically to less than 5% by weight of residual carbon in the fly ash, are desirable in large, multi-burner utility boilers fired with pulverised coal in order to optimise plant efficiency and allow the ash to be incorporated in building materials. Achieving high levels of char burnout can be a particular problem with air-staged low-NO_x combustors, where air/fuel ratios (and flame temperatures) have to be constrained to give satisfactory emission levels. Switching to imported low-sulphur coals can also be associated with a need to at least assess the potential for burnout problems.

In general the levels of carbon in ash required represent very high overall fuel conversion. For example, a coal with 10%w/w ash dry basis giving 5% carbon in ash will still achieve 99.4% conversion. The difference between satisfactory and unsatisfactory burnout thus depends on whether a very small fraction of the coal does or does not burn. Due to the heterogeneous nature of pulverised coal the properties of this 'least likely to burn' (LLB) fraction could well differ from the bulk properties of the whole coal. Consideration of heat and mass transfer would suggest that larger particles make up the bulk of the LLB fraction, and particularly those larger particles which form less reactive chars. In contrast to this material, which might be classed as being unlikely to burn because it is inherently 'bad', there is also a strong likelihood that some coal particles do not burn because they are 'unlucky'. Particles which enter through burners which, because of poor fuel distribution, have a lower than average air/fuel ratio fall into this latter category, especially if they also enter in an upper row of burners or adjacent to a wall.

Previous work by one of the authors has confirmed the heterogeneous nature of pulverised coals by showing that combusting coal particles exhibit a range of reactivities, and that average reactivities decrease with increasing conversion¹. A band of reactivities has also been observed in chars collected from utility boiler fly ash, with a general trend for char reactivity to reduce with increasing particle size². Even at relatively high levels of conversion (~ 50%) chars produced in a laboratory entrained flow reactor (EFR) still had significantly higher reactivity than utility fly ash chars from the same coal³.

The deactivation of coal chars obviously has considerable implications for interpreting char burnout behaviour in itself, but why it occurs is not clear. One explanation is that, with a heterogeneous coal and hence char, the components which are inherently more reactive are burnt preferentially leaving a residue of less-reactive material. Another mechanism, which may either dominate or operate in parallel, is that even at the short particle residence times occurring in utility boilers (~2 seconds) thermally-induced heteroatom loss and/or structural reordering in the chars have occurred, with a consequent reduction in the number of active sites. High resolution transmission electron microscopy in fringe image mode has confirmed that chars from utility boilers are indeed more ordered than chars from the EFR³, but this may reflect either heterogeneity in the parent coal plus differences in degree of conversion, or differences in peak particle temperature and residence time (>1800°C vs. ~1570°C, ~1s vs. ~100 ms respectively).

In order to promote an understanding of the relative importance of the two mechanisms, this study examines the effect of time/temperature history on char reactivity. A recently-developed wire mesh (WM) apparatus was used to achieve char temperatures up to 1800°C with, unlike entrained flow apparatus, essentially no constraint on particle heating times. Since heating takes place under inert gas (helium) any effects due to selective oxidation are avoided. The work formed a preliminary stage in a larger project which will also examine the effect of coal heterogeneity in more detail.

EXPERIMENTAL METHODS

Fly ash samples containing char for analysis were obtained from plant trials. Pulverised coal samples were either sampled on plant or prepared from corresponding lump coal. All coal samples were dry sieved to give a 125-150µm size cut for WM analysis. This was dried overnight in a nitrogen-purged oven at 105°C and stored under nitrogen until required. Char samples were obtained from fly ash either by sieving to give a carbon-enriched size cut >150µm, or by particle density segregation in a sub-fluidised bed.

Coal samples were charred using a high-temperature WM reactor developed at Imperial College. The sample (~10mg) is held between layers of folded molybdenum wire mesh which also act as an electrical resistance heater. Heating currents of up to 2000 A are provided under computer control from a 24 V DC source, with a two-colour pyrometer for temperature measurements. A helium gas sweep flows across the mesh (at atmospheric pressure) to remove volatile products. A more detailed description of the apparatus will be published elsewhere⁴. Char samples for two of the coals were also prepared in an entrained flow reactor at Sandia National Laboratory in 12% oxygen at a gas temperature of 1327°C, peak particle temperatures of 1570°C, and residence times from 47 to 234 ms.

Char reactivities were compared using thermogravimetric analysis (TGA). Samples were heated in a PL Thermal Sciences TG760 series TGA to 900°C at 15 K/min in 7% oxygen in nitrogen. This reduced oxygen concentration eliminates 'ignition peaks' (uncontrolled autothermal combustion within the char sample) that can occur if the sample is heated in air. Char samples were ground to <10µm to eliminate any effects due to particle size. Although this technique utilises standard commercial equipment some development work was required to achieve consistent, repeatable results with small samples (2-3mg).

TGA data logging and analysis were carried out using in-house software. The instantaneous sample mass was monitored as the sample was heated. Sample temperature was measured using a thermocouple positioned 0.7 mm under the crucible. Results were expressed as burning profiles (rate of weight loss versus sample temperature), or as Arrhenius plots (logarithmic reaction rate against inverse temperature). This non-isothermal characterisation technique has several advantages over isothermal methods (e.g. time for 50% burnoff). In isothermal char reactivity tests the char must be first heated to the desired temperature in inert gas, before switching to the desired oxygen concentration. Data for the intermediate oxygen levels during switchover periods, which can represent a considerable portion of the total burnoff at elevated temperatures, cannot then be used. Analysis times will also vary significantly at a given temperature with the range of char reactivities encountered in char combustion studies (e.g. low reactivity chars may require a number of hours for 50% conversion at 500°C in 7% O₂). Errors in sample temperature measurements may, however, be worse in non-isothermal analysis due to differential heating, particularly if (as in this case) the thermocouple is not placed in direct contact with the sample.

RESULTS AND DISCUSSION

The variation in reactivity for chars prepared from Illinois #6 coal by different methods is shown as an Arrhenius plot in Fig. 1. As noted already, chars from the EFR have significantly higher chemical reactivities than the utility boiler fly ash chars. Chars obtained after heating in the WM reactor at 1600°C are also significantly more reactive. The reactivity of the WM chars decreases with increased hold time at peak temperature, but even at 10 s hold the 1600°C WM char is more reactive than the fly ash char. The Arrhenius plot line for a WM char obtained with a peak temperature of 1800°C and a residence time of 2 s, however, intersects the Arrhenius plot line for the utility char, being apparently less reactive at low conversions in the TGA but more reactive at higher conversions. Similar trends for the WM chars as compared with the fly ash chars were also observed for a South American coal (Fig. 2) and US Daltex coal (Fig. 3), although this last coal appears to be particularly susceptible to thermal deactivation.

An interesting feature of Figs 1 to 3 is the difference between apparent activation energies for WM and fly ash chars. Both exhibit reasonably straight lines on the Arrhenius plots over the range 5% to 95% conversion (signal/noise ratio makes interpretation difficult at higher conversions), suggesting modelling by a familiar first order reaction rate expression for loss of sample weight, W , of the form:

$$dW/dt = -a.W.e^{-E/RT}$$

For the WM chars, increased heating severity changes the pre-exponential factor, a , but not the activation energy, E , suggesting that the number, but not the type, of active sites is being affected. The lower apparent activation energy for the fly ash chars might then be taken as an indication of the presence of a significantly different type of char, perhaps due to selective oxidation.

If, however, the WM and fly ash chars are in fact different types, it might be considered an unusual coincidence that overall reactivities are still comparable for the similar peak temperatures. This observation is explored in more detail in Fig. 4, which shows the TGA burning profile that would be obtained for a hypothetical heterogeneous char with a single activation energy, but a normal distribution of pre-exponential factors (the WM char data show that this could, for example, be obtained by subjecting a batch of coal particles to a range of different time/temperature histories during devolatilisation). The Arrhenius plot line for 5% to 95% conversion for the modelled TGA burning profile is still extremely linear (correlation coefficient of 0.997), but the heterogeneity has the effect of reducing the apparent activation energy from an assumed 175 kJ/kmole to 145 kJ/kmole.

Since particles in a utility boiler will have experienced a range of time/temperature histories it appears plausible that this, at least partly, accounts for the apparently lower activation energies for fly ash chars shown in Figs 1 to 3. If temperature alone is responsible, then it can further be concluded that the fly ash chars have experienced temperatures both above and below 1800°C. This scenario corresponds with the LLB fraction being made up of particles that are simply 'unlucky'.

The very low reactivities of fly ash chars at higher conversion levels in the TGA compared to 1800°C WM chars suggest, however, that extremely high particle temperatures would have to have occurred to account for all of the differences observed. Some additional char heterogeneity due to differences between the parent coal particles therefore seems likely. This pulverised coal heterogeneity may be in the organic fraction or in the catalytic properties of the mineral matter for graphitisation and/or oxidation. In either case, the LLB fraction would then consist, at least in part, of particles that were inherently 'bad'.

It is also worth considering to what extent the original WM coal samples are themselves heterogeneous in this way. In this case even the higher apparent activation energies observed for the WM chars could still be an underestimate, with considerable implications for extrapolating low-temperature TGA data to boiler combustion temperatures.

CONCLUSIONS

Char oxidation reactivity reduces progressively with increased temperature and hold time under conditions encountered in pulverised coal combustion. At elevated temperatures (1800°C) char reactivities obtained by heating alone approach fly ash residual char reactivities.

Fly ash residual char from utility boilers is probably heterogeneous in its reactivity. If some of the char particles have experienced temperatures well in excess of 1800°C then temperature alone could explain this heterogeneity, otherwise heterogeneity in the original coal plus loss of more reactive material, or catalysis of oxidation or char graphitisation by mineral matter, must also be occurring.

Char reactivities measured by non-isothermal TGA methods are likely to give correct relative trends, but apparent activation energies may not be reliable due to char heterogeneity (and possibly also temperature offsets).

ACKNOWLEDGEMENTS

The authors would like to acknowledge financial support for this work from the UK Science and Engineering Research Council, the British Coal Utilisation Research Association, the UK Department of Trade and Industry through ETSU, National Power PLC, and the US Department of Energy.

REFERENCES

1. Hurt, R.H., *Energy & Fuels* 7, 1993, 721-733.
2. Gibbins, J.R. & Williamson, J., *Proc. 7th ICCS, Banff, Sep. 1993*, paper PS1.9.
3. Hurt, R.H., Yang, N.Y.C., Headley, T.J. & Gibbins, J.R., *Proc. 7th ICCS, Banff, Sep. 1993*, paper OS12.2.
4. Pendlebury, K.J., Man, C.K. & Gibbins, J.R., *Rev. Sci. Instrum.*, (in preparation).

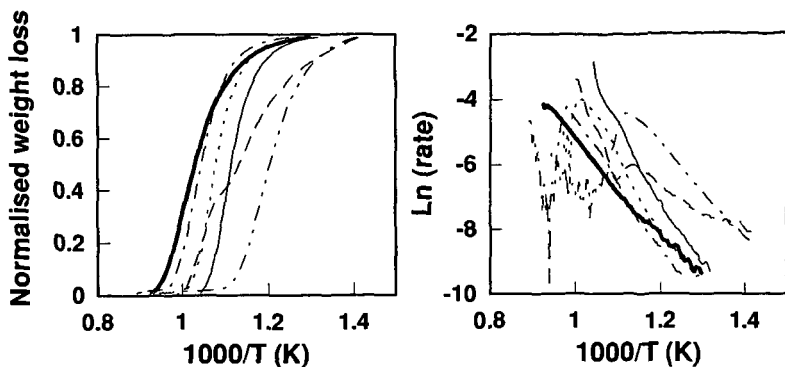


Figure1 TGA sample weight and reaction rate as a function of inverse temperature for Illinois #6 chars

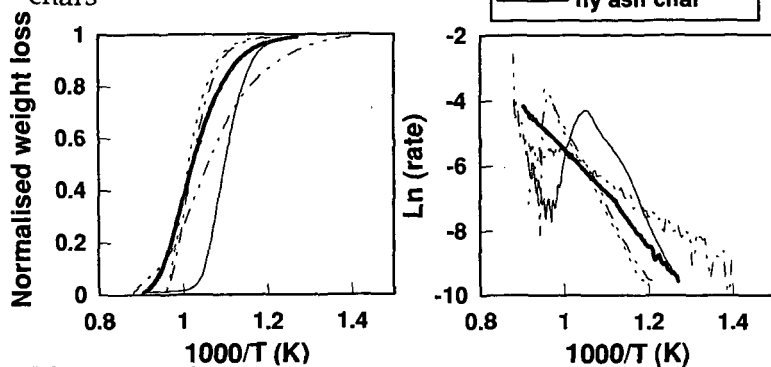


Figure 2 TGA sample weight and reaction rate as a function of inverse temperature for South American coal chars

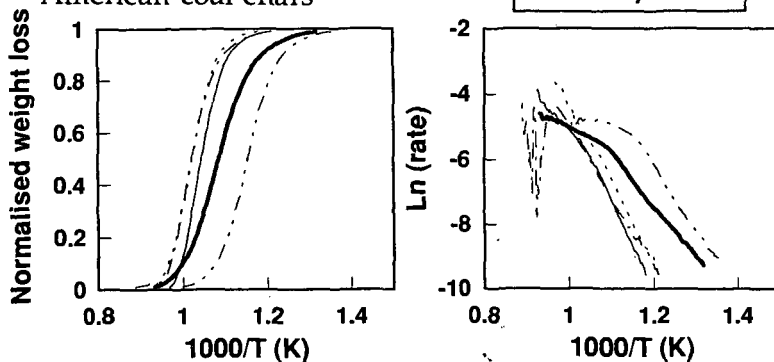


Figure 3 TGA sample weight and reaction rate as a function of inverse temperature for Daltex chars

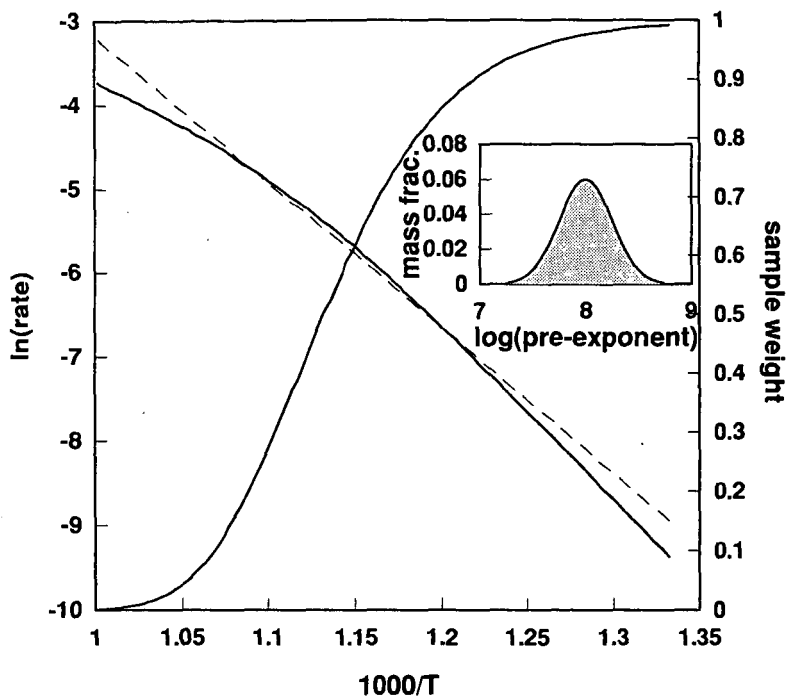


Figure 4 Effect of char heterogeneity on apparent activation energy

A PRIORI SIMULATION OF COAL PYROLYSIS EXPERIMENTS BASED ON COAL ELEMENTAL COMPOSITIONS

Yuxin Zhao, Michael A. Serio, and Peter R. Solomon
Advanced Fuel Research, Inc.
87 Church Street, East Hartford, CT 06108, U. S. A.

Keywords: Coal Pyrolysis, Modeling, Tar Yields.

INTRODUCTION

Coals come in various ranks and from different geological origins. Substantially different characteristics are commonly observed for coals of different ranks. Coal samples from the same seam can exhibit large variations in their devolatilization and related thermal and combustion behavior. Such variations have large impacts to the design and operating conditions of coal combustion systems. It is imperative that coals are well characterized before their utilization. This normally requires sophisticated instrumentation and special expertise, which are not likely available in a single laboratory. Robust methods of predicting coal devolatilization behavior before invoking expensive experiments can be of practical importance.

Recently, there have been developments of several coal devolatilization models [1-6], which have various capabilities of predicting coal thermal decomposition under practical conditions. A common shortcoming of these models is that they require a large set of data input, including kinetic parameters, gas precursor compositions and additional parameters describing the coal polymeric structure. These input data must be generated based on a series of experimental measurements for each coal of interest. Predictions are limited to coals that have been studied. This limitation has long been criticized although it originates from the complicated nature of the coal structure. On the other hand, some investigators have tried to correlate the devolatilization properties to the coal types. For instance, Ko et al. [7] and Neavel et al. [8] have developed methods of predicting the upper bound of tar yields, X_{tar} , from coal elemental compositions. The predicted X_{tar} can be used as an input parameter of general tar kinetic models such as those developed by Serio et al. [9] and Suuberg et al. [10]. Niksa and Kerstein [11,12] have also proposed a correlation method for the FLASHCHAIN coal devolatilization model which predicts tar and the total volatile yields in pyrolysis based on ultimate analysis.

This paper presents a general method that provides a direct correlation between coal elemental compositions and the input parameters of a general coal devolatilization model, FG-DVC [1-3], which can predict, in addition to the tar and total volatile yields, the yields of individual gas species, the tar molecular weight distribution, and the char fluidity. This model was validated for the eight Argonne Premium coals based on measurements of pyrolysis kinetics from TG-FTIR analysis, solvent extraction and solvent swelling to measure extractables and initial crosslink density, respectively, Gieseler plastometer experiments to measure fluidity, pyrolysis-FIMS to measure the tar molecular weight distribution and ultimate analysis to determine the elemental compositions (C, H, N, S, O) [3]. The large number of experimental inputs allowed the development of a model which can make detailed predictions of coal devolatilization, as indicated above. However, this feature presented a difficulty when applying the model to unknown coals. The correlation method presented in this paper enables us to apply the FG-DVC model to coals of a wide range of types without prior knowledge of them except the elemental analysis, and supports our contention that the FG-DVC model is a general model that can perform expeditious evaluations of coal thermal decomposition under many heating and pressure conditions. This correlation approach in its preliminary form has been implemented into a 2-dimensional coal combustion model, PCGC-2 [13]. After a description of the method, the model predictions are compared with tar yield data collected at fast heating rates and various pressures from the literature [7, 14-21], and with tar yields at slow heating rates measured with TG-FTIR analysis in our laboratory.

BACKGROUND

FG-DVC [1-3] is a general coal devolatilization model that predicts coal thermal decomposition into light gases, tar and char. It also predicts other related property changes, i.e., coal viscosity and swelling, during pyrolysis. Recent improvements of this model have given it the ability to predict gaseous sulfur and nitrogen species evolved during pyrolysis [22]. The following is just brief description of this model, as the details have been published elsewhere [1-3, 22,23].

Coal has a very complicated structure, which is essentially a mixture of an aromatic matrix, side chain components and some loose fragments. The thermal decomposition of the coal structure involves many parallel and competitive processes. In modeling these

processes, FG-DVC uses two submodels. The FG model simulates the thermal evolution of various functional groups and the DVC model predicts the depolymerization, vaporization and crosslinking processes occurring in the coal polymer network. In the FG submodel, the gas evolution from functional group precursors is modeled with parallel first order differential equations and a distributed activation energy formulation is used to reflect the diversity of coal structures. The thermal evolution of the coal polymer matrix is modeled with a network model [2], which consists of nodes and the connections between them. The nodes represent the polymer clusters and there are two types of connections between them, i.e., bonds and crosslinks. At elevated temperatures, there is a competition between bond breaking and crosslinking. The properties of the network are fully determined by these two competing processes through percolation theory [24]. The most important property of the network is the molecular weight distribution of the clusters. The heavy molecules remain in the condensed phase to become char, while the light ones evaporate to become tar. The vaporization is calculated based on a mechanism given by Fletcher [25]. The tar rate is further limited by internal transport, which is assumed to be controlled by the total rate of gas species evolution plus the light tar [1]. This mechanism enables the model to predict the pressure variation of tar yields.

Input parameters are required to describe the coal structure and its evolution kinetics. Sets of parameters have been developed for the eight coals provided by the Argonne Premium Coal Sample Program [26], employing various analytical methods, including TG-FTIR, solvent swelling and extraction, fluidity, NMR, and FIMS.

CORRELATION APPROACH

The behavior of coal when subjected to a physical and chemical analysis or treatment exhibits rank dependence in most instances. For example, Solomon et al. [3] have shown a consistent variation of coal functional group compositions with rank. The basis of the correlation formulation presented here relies on the well-known van Krevelen diagram [27], which indicates that the progress of coalification in terms of the coal's atomic hydrogen to carbon (H/C) and oxygen to carbon (O/C) ratios forms a distinctive band in the H/C and O/C two dimensional plane. Each coal has a coordinate (O/C, H/C) in the van Krevelen diagram. Fig. 1 illustrates the variation of the vitrinite reflectance index (v.r.i.) as a function of H/C and O/C, for 45 PSOC coals sponsored by the U. S. Department of Energy. As v.r.i. is commonly accepted as a rank indicator, it is reasonable to assume that there exists a correlation between rank and elemental composition. Therefore, a parameter for an unknown coal can be interpolated from those for a set of coals that are well-studied. These well-defined coals are called library coals, a term used by Williams [28].

We propose to use a two dimensional linear interpolation method commonly used in finite element analyses, with O/C and H/C as two rank indicators. Let x be a parameter of an unknown coal and $x_0(i)$ ($i=1, N$) are the corresponding parameters of the N library coals. The N library coals form a 2 dimensional triangular element mesh in the van Krevelen diagram as displayed in Fig. 2, where N is 9 with each node representing a coal. The mesh nodes are plotted as filled circles and other symbols in the plot are the coals to be interpolated. Each triangle element contains three nodes (coals). If an unknown coal is inside the element J , whose three nodal numbers are $i^{(1)}_J$, $i^{(2)}_J$, and $i^{(3)}_J$, the unknown parameter, x , is interpolated as

$$x = (1-r-s) \cdot x_0(i^{(1)}_J) + r \cdot x_0(i^{(2)}_J) + s \cdot x_0(i^{(3)}_J) \quad (1)$$

where r and s ($0 \leq r, s \leq 1$) are the local coordinates of the unknown coal in element J and are determined from the positions of the unknown coal and the three interpolating coals in the van Krevelen diagram. Let U denote the point of the unknown coal in the van Krevelen diagram. $\Delta(i^{(1)}_J, i^{(2)}_J, i^{(3)}_J)$, $\Delta(i^{(1)}_J, U, i^{(3)}_J)$, and $\Delta(i^{(1)}_J, i^{(2)}_J, U)$ are the areas of the triangles formed by nodes $(i^{(1)}_J, i^{(2)}_J, i^{(3)}_J)$, $(i^{(1)}_J, U, i^{(3)}_J)$, and $(i^{(1)}_J, i^{(2)}_J, U)$, respectively. r and s are calculated as follows

$$\begin{aligned} r &= \frac{\Delta(i^{(1)}_J, U, i^{(3)}_J)}{\Delta(i^{(1)}_J, i^{(2)}_J, i^{(3)}_J)} \\ s &= \frac{\Delta(i^{(1)}_J, i^{(2)}_J, U)}{\Delta(i^{(1)}_J, i^{(2)}_J, i^{(3)}_J)} \end{aligned} \quad (2)$$

The interpolation mesh is composed of nine coals, six of which come from the Argonne Premium Coal Sample Program and three of which are PSOC coals (PSOC 1474, PSOC 1448, and PSOC 1521). Extensive experimental studies have been carried out on the Argonne Premium Coals and the model input parameters are well established [3].

Predictions of the pyrolysis yields of these coals under various conditions are in very good agreement with the data collected in many types of reactors [29]. The Lewiston-Stockton coal was not used because it has a very similar elemental composition to the Pittsburgh Seam Coal. The Pocahontas #3 coal was not selected since it is of substantially high rank and is far away from the rest of the coals. Three PSOC coals were added to this mesh recently, so that a larger area is covered. The functional group compositions and the pyrolysis evolution kinetic parameters of these three coals were obtained based on data from TG-FTIR analysis and solvent extraction experiments performed recently in our laboratory and fluidity data from the PSOC coal data base.

With this scheme, any of the model parameters for the FG-DVC model can be interpolated for an unknown coal when its elemental composition is identified. Special caution must be used in interpolating the functional group compositions of the oxygen, sulfur and nitrogen gases in order to maintain a proper mass closure. For example, the total amount of the oxygen containing functional groups is limited by the oxygen content. Therefore, instead of interpolating the amounts of oxygen gas precursors directly, only the fraction of oxygen in a functional group is calculated and is used to compute the amount of this functional group from the oxygen content. The same procedure is followed for the sulfur and nitrogen gases.

TAR YIELD PREDICTIONS

Tar composes up to about 50% of the total volatiles during coal combustion for most coals. The secondary reaction of tar in the system produces soot, PAH, and light gases that affect ignition, flame stability and the radiative property of the flame. Tar yields vary with coal type and are affected by reactor conditions such as pressure and heating rate. The interpolation scheme presented above enables the FG-DVC model to predict the tar yield of a coal from its elemental analysis under various pressure and heating rate conditions. To verify this capability, tar yield data were assembled from literature and were compared with the model predictions. These data were measured with heated grid systems under fast devolatilization (heating rates from 100 °C/s to 1000 °C/s) for various coals and pressures (10^{-4} to 7 MPa). In addition to these data, tar yields from eight PSOC coals were measured with a TG-FTIR system at heating rate of 30 °C/min and atmospheric pressure. The details of the TG-FTIR system have been presented elsewhere [30]. The data used for model verification were selected to span a wide range of coal types, from lignite to low volatile bituminous, and pyrolysis conditions. Part of the data set was taken from the tabulation given by Ko et al [7].

For each of these coals, the FG-DVC input parameters were interpolated with the scheme proposed above and the tar yields from these coals were predicted with the pressures and the heating rates specified in these references. Eleven coals from the references and the eight PSOC coals are inside the mesh and the standard interpolations were performed. The Pocahontas, Illinois #6 and North Dakota lignite studied by Suuberg et al. [17] are outside the mesh and were predicted with the input parameters of the corresponding Argonne coals. The Alabama bituminous coal studied by Freihaut and Seery [15] and the Beulah Zap coal studied by Ko et al. [7] were predicted based on input files used for the Argonne Upper Freeport coal and Zap lignite, respectively. The Colstrip lignite by Reitzen [21] is close to the edge of the triangle formed by Zap lignite, Wyodak, and Illinois #6 coals, and was modeled with an elemental composition inside this triangle and closest to Colstrip.

The predictions and the data are compared in Fig 3. The standard errors of the estimates are 3.84%, 3.12%, and 3.38% for data collected at vacuum, atmospheric and high pressures, respectively. The total standard error of the estimate is 3.35%. This is in the same range of experimental scatter commonly encountered in tar measurements. The standard error of the estimate, σ , is calculated as follows:

$$\sigma = \sqrt{\sum_{i=1}^N \frac{(Y_i^m - Y_i^p)^2}{N}} \quad (3)$$

where Y_i^m and Y_i^p are the measured and predicted tar yields, and N is the number of data points compared.

Fig. 4 compares the predicted and the measured variations of tar and total volatile yields as a function of heating rate for a Linby coal studied by Gibbins and Kandiyoti [20]. For an Illinois #6 coal studied by Cai et al. [19], the variations of tar and total volatile yields as a function of heating rate and pressure were predicted and are compared with the data [19] in Fig. 5. These plots show that the predictions are in a reasonably good agreement with the data. It should be noticed that this is achieved based only on the elemental compositions

without further prior knowledge of these coals.

DISCUSSION

The success of this interpolation scheme depends on a thorough understanding of the library coals. Selection of these library coals must be performed with care so that none of these coals has peculiar behavior and deviates from coals in its rank. Although the current mesh contains only nine coals, it is one advantage of this method that it can be easily extended to include more coals. Adding more coals in the interpolation mesh will certainly increase the reliability of the predictions and will allow coverage of a wider range of coal types.

A few large discrepancies were observed for some coals, indicating needs for further improvements. Under-predictions of tar yields in vacuum were seen for a group of Pittsburgh seam coals, for which the measured tar yields are 39.0% [15], 37.0% [10] and 37.7% [18] and the predicted vacuum tar yields are 33.0%, 29.2% and 32.6%, respectively. However, good agreement was obtained at atmospheric pressure for these coals (26.5% [10] vs. 24.5% and 26.5% [17] vs. 26.9). Since the pressure variations are correctly predicted for other coals, the high vacuum tar yields for the Pittsburgh seam coals appear to be caused by a mechanism particular to these coals. The model also under-predicts tar yields for PSOC 1519 and 1492 coals. The Sesser sub-bituminous coal studied by Ko et al. [14] is the only coal that has a large over-predicted atmospheric tar yields (21.5% [14] vs. 27.0%). This coal seems to be an unusual coal as a relatively low tar yield was also reported by Reitzen [21] (11%). For most of the coals the predictions are within 3% of the data and the standard error of estimation calculated without the above large discrepancies is 2.54 wt%.

The basis of this interpolation method is the assumption that coals within the same rank behave similarly. Predictions based on this method are targeted at the normal or mean behavior of coals within the same rank. Deviations from normal, however, should be expected. If the deviation is large and can not be identified with an existing mechanism, the behavior of coals becomes unpredictable with the current method. The comparisons presented in Figs. 3 to 5 indicate that, for most coals, the deviations are small enough that the tar yields are well predicted. Some improvement may be achieved by including one additional parameter, such as the volatile matter content, in the correlation.

The yields and the compositions of the volatile gases are also important. The capability of FG-DVC in predicting the total volatile yields has been demonstrated in Figs. 4 and 5. The amounts of individual gas species are also predicted by FG-DVC along with the tar yields and this is one of the chief advantages of this model. However, comparisons are more difficult because of the relatively small amount of available data. This will be the subject of further studies.

CONCLUSIONS

An interpolation method was proposed to correlate the input parameters of a coal devolatilization model, FG-DVC, for untested coals, and is conceptually applicable to other devolatilization models. This method uses a set of well defined coals (library coals) to form a triangular mesh in the van Krevelen diagram. If an unknown coal is within a triangle formed by three library coals, the model input parameters for this unknown coal can be interpolated from those of the three library coals based solely on a knowledge of the elemental composition. This method allows the FG-DVC model to be used for any coal that can be interpolated. It is also easy to accommodate more library coals, so that a wider range of coal types can be covered.

The validity of this method was demonstrated by comparing the tar yields measurements and predictions for 27 coals under a wide range of pressures and heating rates. For most of the coals, the predictions compare very well with the data.

ACKNOWLEDGMENTS

This work was supported by the Morgantown Energy Technology Center of the US Department of Energy, through contract DE-AC21-86MC23075. The authors also wish to acknowledge helpful comments from Professor Eric M. Suuberg of Brown University.

REFERENCES

1. Solomon, P. R., Hamblen, D. G., Carangelo, R. M., Serio, M. A., and Deshpande, G. V., *Energy & Fuels*, 2, 405 (1988).
2. Solomon, P. R., Hamblen, D. G., Yu, Z. -Z. and Serio, M. A. *Fuel*, 69, 754 (1990).
3. Solomon, P. R., Hamblen, D. G., Serio, M. A., Yu, Z. -Z. and Charpenay, S. C., *Fuel*, 72, 469 (1993).
4. Grant, D. M., Pugmire, R. J., Fletcher, T. H., and Kerstein, A. R., *Energy & Fuels*, 3,

- 175 (1989)
5. Reynolds, J. G., and Burnham, A. K., submitted to *Energy and Fuels*, 1992.
6. Niksa, S., *AIChE J.*, 34, 790 (1988).
7. Ko, G. H., Sanchez, D. M., Peters, W. A. and Howard, J. B., Twenty-Second Symp. (Intl) on Comb., p. 115, The Combustion Institute, Pittsburgh, 1988.
8. Neavel, R. C., Smith, S. E., Hippo, E. J., and Miller, R. N., *Proc. of Intl. Conf. on Coal Sci.*, p.1, Dusseldorf, Sept. 1981.
9. Serio, M. A., Peters, W. A., and Howard, J. B., *I & EC Res.*, 26, 1831 (1987).
10. Suuburg, E. M., Peters, W. A., and Howard, J.B., 17th Symposium (Int.) on Combustion, The Combustion Institute, Pittsburgh, PA pp. 117-130 (1979).
11. Niksa, S. and Kerstein, A. R., *Am. Chem. Soc. Div. Fuel Chem. Preprints*, 38(4), 1346 (1993).
12. Niksa, S. and Kerstein, A. R., proceedings of the Intl Conf. on Coal Sci., pp. 397-400, (1993).
13. 93-PCGC-2, Users Manual, Brigham Young University and Advanced Fuel Research, Inc., 1993.
14. Ko, G. H., Peters, W. A. and Howard, J. B., *Fuel*, 66, 1118 (1987).
15. Freihaut, J. D. and Seery, D. J., *Am. Chem. Soc. Div. Fuel Chem. Preprints*, 26(2), 133 (1981).
16. Arendt, P. and van Heek, K-H., *Fuel*, 60, 779 (1980).
17. Suuberg, E. M., Unger, P. E., and Larsen, P. E., *Energy & Fuels*, 1, 305 (1987).
18. Suuberg, E. M., Lee, D. and Larsen, J. W., *Fuel*, 64, 1668 (1985).
19. Cai, H. -Y., Güell, A. J., Dugwell, D. R. and Kandiyoti, R., *Fuel*, 72, 322 (1993).
20. Gibbins, J. R. and Kandiyoti, R., *Fuel*, 68, 895 (1989).
21. Reitzen, T. R., Effects of Pyrolysis Conditions on Products of Interests in Formed Coke Production, M. S. thesis, Massachusetts Institute of Technology, 1978.
22. Basilakis, R., Zhao, Y., Solomon, P. R., and Serio, M. A., *Energy & Fuels*, 7, 710 (1993).
23. Hamblen, D. G., Yu, Z. Z., Charpenay, S., Serio, M. A., *Proc. of Intl. Conf. on Coal Sci.*, pp. 401-404, (1993).
24. Stauffer, D., and Aharony, A., *Introduction to Percolation Theory*, 2nd Edition, Taylor & Francis, London, UK, 1991.
25. Fletcher, T. H., Kerstein, A. R., Pugmire, R. J., Solum, M. S., and Grant, D. M., *Energy & Fuels*, 6, 414 (1992).
26. Vorres, K. S., *Energy & Fuels*, 4(5), 420 (1990).
27. van Krevelen, D. W., *Coal*, 3rd Edition, Elsevier Publishing Company, Amsterdam, 1993.
28. Williams, A., Pourkashanian, M., Bysh, P. and Norman, J., Keynote address to the Coal Utilization and the Environment Conf., May 18-20, 1993, Orlando, U. S. A.
29. Serio, M. A., Solomon, P. R., Yu, Z. -Z., Deshpande, G. V., and Hamblen, D. G., *Am. Chem. Soc. Div. Fuel Chem. Preprints*, 33(3), 91, 1988.
30. Solomon, P. R., Serio, M. A., Carangelo, R. M., Basilakis, R., Gravel, D., Baillargeon, M., Baudais, F., Vail, G., *Energy & Fuels*, 4, 319 (1990).

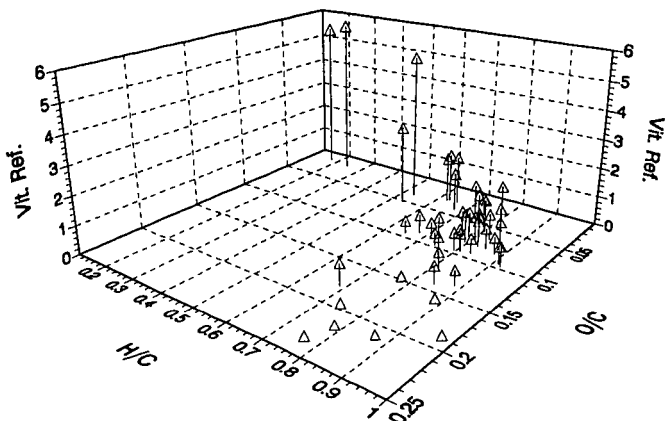


Figure 1. Variation of Vitrinite Reflectance of Coals from the PSOC DOE Sample Bank as a Function of H/C and O/C Ratios in the van Krevelen Diagram.

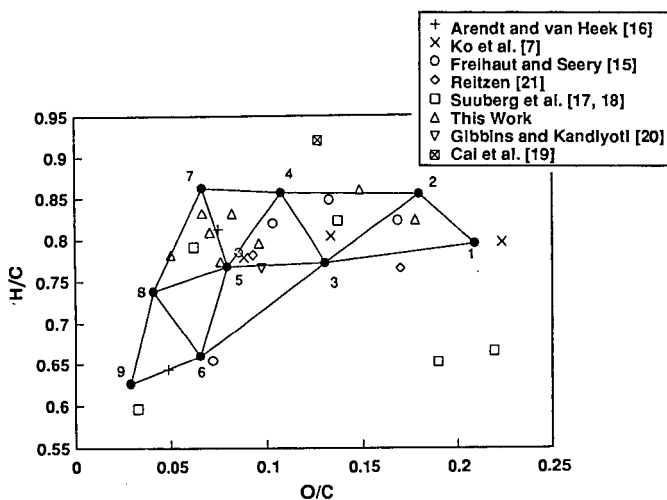


Figure 2. The Interpolation Mesh in the van Krevelen Diagram and Coals Used for Tar Yield Comparison. Argonne Coals: (1) Beulah Zap; (2) Wyodak; (3) Illinois #6; (4) Blind Canyon; (5) Pittsburgh #8; (6) Upper Freeport. PSOC Coals: (7) PSOC 1448; (8) PSOC 1474; (9) PSOC 1521.

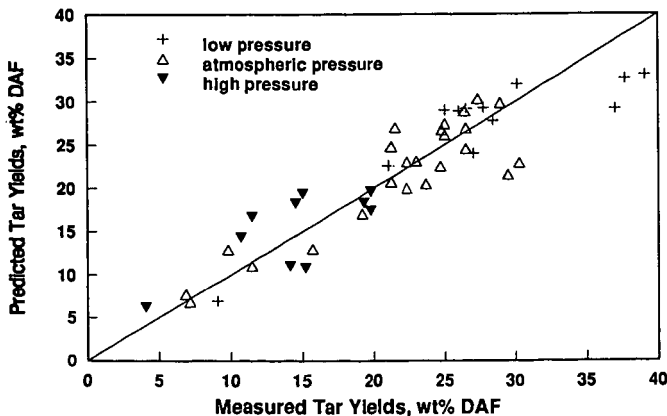


Figure 3. Comparison of the Measured and the Predicted Tar Yields for Coals Given in Fig. 2.

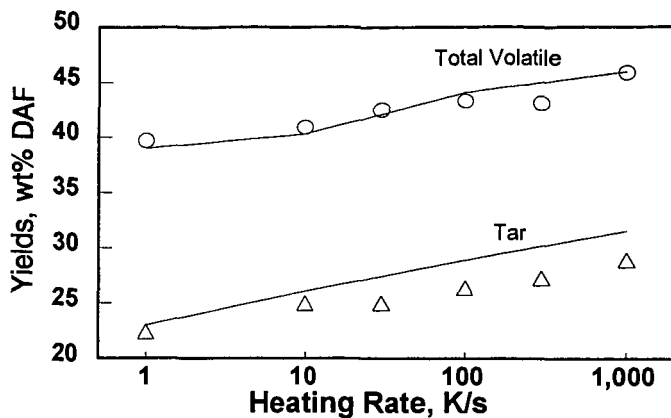


Figure 4. Variations of Tar and Total Volatile Yields as a Function of Heating Rate for a Linby Coal Studied by Cai et al. [19]. The Lines are Predictions and the Symbols are the Data.

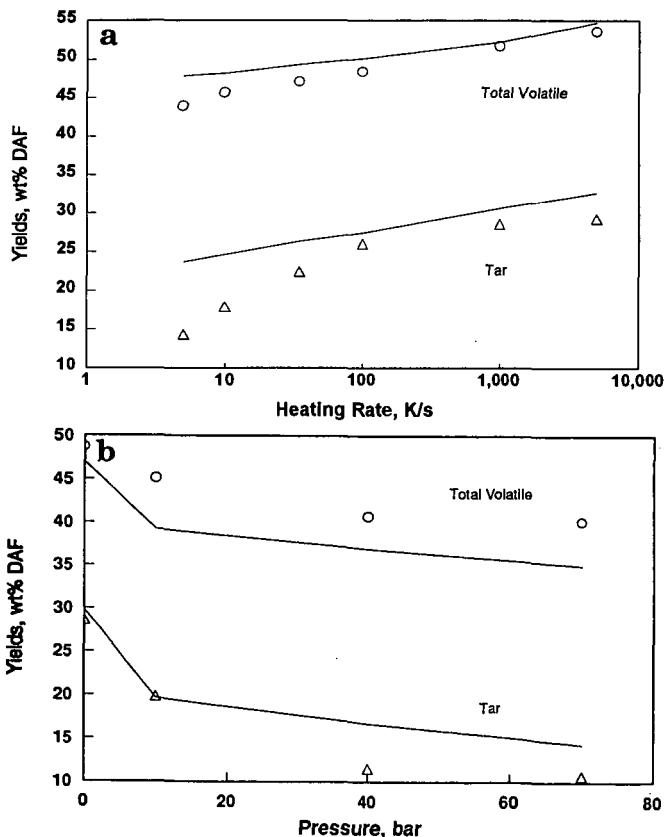


Figure 5. Variations of Tar and Total Volatile Yields as a Function of a) Heating Rate and b) Pressure for a Linby Coal Studied by Cai et al. [19]. The Lines are the Predictions and the Symbols are the Data.

STUDIES OF THERMAL AND CATALYTIC HYDROLIQUEFACTION OF MODEL COMPOUNDS, WASTE POLYMERS AND COAL BY HIGH PRESSURE TG/GC/MS

Kui Liu, Emma Jakob, Włodzimir Zmierzak*, Joseph Shabtai* and Henk L.C. Meuzelaar
Center for Micro Analysis & Reaction Chemistry
*Department of Chemical and Fuels Engineering
University of Utah, Salt Lake City, UT, 84112

KEYWORDS: high pressure TG/GC/MS techniques; catalytic hydrolypyrolysis mechanisms; coal/waste polymer co-processing

INTRODUCTION

A recently developed on-line high pressure thermogravimetry (TG)/gas chromatography (GC)/mass spectrometry (MS) system [1] provides certain advantages over other on-line analysis techniques for high pressure reactors reported previously [2,3]. The high pressure TG/GC/MS system enables the simulation of solvent-free thermal and catalytic reactions for polymers and coal. During the reactions the total weight change is monitored and the volatile intermediate products are identified. It requires only very small amounts (10-100 mg) of sample and can be operated at high pressure under different atmospheres (N_2 , He, H_2 , etc.). Current efforts to recycle lower grade postconsumer polymers such as colored polyethylene and polystyrene or used rubber tires, are concentrated on co-processing with coal [4-6]. Purely thermal degradation processes involve both decomposition and condensation (recombination) reactions and the resulting product is highly olefinic and often aromatic. In order to improve the yield and selectivity of the process, a great deal of effort has been spent on finding the proper catalysts. Catalysts selected for the present studies include ZrO_2/SO_4^{2-} , $(NH_4)_2MoS_4$ and carbon black. Carbon black present in waste rubber tires has been reported to be very selective for the cleavage of specific alkylaryl bonds [7]. $(NH_4)_2MoS_4$ has been shown to improve the liquid yields in coal liquefaction [8]. The superacid catalyst Zr_2O_7/SO_4^{2-} possesses markedly higher hydrogenolytic activity compared to that of conventional SiO_2 -supported soluble Fe salts [9].

EXPERIMENTAL

Experiments with a styrene-butadiene rubber (SBR; nonvulcanized) sample in the presence of various catalysts (carbon black, $(NH_4)_2MoS_4$ and ZrO_2/SO_4^{2-}) and coprocessing runs of coal and polymers (polyethylene, polystyrene, waste rubber tire, commingled plastic mixture) were conducted in a high pressure TG/GC/MS system at a hydrogen pressure of 900 psi. The experimental procedure and schematic of the equipment were described in detail in a previous paper [1]. The styrene-butadiene rubber (SBR) (30% polystyrene, 20 mesh), polystyrene (MW 45000, -100 mesh), polyethylene, carbon black (Black Pearl 2000) and $(NH_4)_2MoS_4$ were obtained from Aldrich Chemical Company. The superacid catalyst ZrO_2/SO_4^{2-} was prepared as reported by Shabtai et al. [9]. In the case of commingled postconsumer plastic, the plastic bottles and containers were washed to remove contaminants and labels before sizing and shaving. Final size reduction was done by grinding in a K-TEC kitchen mill. A high volatile bituminous coal (DECS-6, Blind Canyon, Utah, obtained from the Penn State Coal Sample Bank) was used in a 1:1 mixture ratio with both model and waste polymers.

RESULTS AND DISCUSSION

The thermal and catalytic reactions of a styrene-butadiene rubber (SBR) polymer as a model compound of rubber tire were studied in a high pressure thermobalance at a hydrogen pressure of 900 psig. As shown by the weight loss profiles in Figure 1, the 10% superacid ZrO_2/SO_4^{2-} catalyst added has little influence upon the rate of decomposition of SBR polymer at a constant heating rate of 10 C/min. However, when the same sample is subjected to a different temperature program using a heating rate of 10 C/min up to 370 C and then kept under isothermal conditions for one hour before being heated up to 500 C at 10 C/min, the effect of the catalyst on the rate of decomposition of SBR polymer is clearly observed (Figure 2). The catalyst greatly increases the rate of degradation of the polymer at 370 C. The results suggest that at a constant heating rate the reactions are dominated by thermal processes so the catalyst effect is not observed. However, the difference between catalytic and thermal processes is brought out effectively at a relatively low isothermal temperature level (e.g., 370 C) chosen to minimize the contribution of thermal reactions.

In addition, the catalytic reactions of SBR with other catalyst types, viz. carbon black and $(NH_4)_2MoS_4$ were studied. In order to compensate for the poor contact between the powdered catalyst and SBR, 10% of catalyst was added to the polymer samples. Comparison of the thermogravimetric curves (Figure 2) shows that the ZrO_2/SO_4^{2-} catalyst increases the weight loss by about 17% at 370 C whereas carbon black and $(NH_4)_2MoS_4$ have no measurable effect on the overall rate of SBR decomposition. As discussed in the literature [9], the ZrO_2/SO_4^{2-} catalyst

causes primarily hydrogenolytic bond cleavage resulting in more weight loss whereas the mild bifunctional catalyst, $(\text{NH}_4)_2\text{MoS}_4$, appears to be ineffective in bond-cleavage reactions. Indeed at the relatively low temperature of 300 C, this catalyst has been found to have little effect on liquids production [8]. The temperature applied in our isothermal experiments is somewhat higher, but the reaction severity is mild due to the very short residence time of the reactants (estimated to be about 15 sec).

Several main product evolution profiles of SBR with various catalysts are shown in Figure 3. The production of benzene is significantly promoted by the $\text{ZrO}_2/\text{SO}_4^{2-}$ catalyst indicating that the solid superacid catalyst has very strong hydrogenolysis activity for α -alkyl-arene bond cleavage. The catalyst contains both the Bronsted acid and the Lewis acid sites [10]. The Bronsted acid sites protonate the aromatic ring and the subsequent α -cleavage results in the formation of benzene and aliphatic compounds. These findings are in agreement with the observation of Shabtai et al. [9] that the $\text{ZrO}_2/\text{SO}_4^{2-}$ catalyst is very effective in the hydrogenolytic α -cleavage of 1,2-dinaphthylethane. The presence of Bronsted acid sites also promotes trans-alkylation reactions between alkylbenzenes and styrene as evidenced by the increased evolution of isomeric methylstyrenes (Figure 3b), ethylstyrene and benzene. The increased yield of styrene (Figure 3c) and α -methylstyrene can be explained by the parallel Lewis acid functionality character of the catalyst. When the Lewis acid sites abstract hydride ions from the benzylic carbons, benzylic carbonium ions are formed. Subsequently, styrene and α -methylstyrene are formed by β -scission of the benzylic carbonium ion. Mild hydrogenation activity of the $\text{ZrO}_2/\text{SO}_4^{2-}$ catalyst was indicated by the increased yield of saturated products such as ethyl benzene (Figure 3d) and isopropylbenzene.

Although, the $(\text{NH}_4)_2\text{MoS}_4$ catalyst does not affect the overall rate of decomposition significantly, some changes in the product composition are observed. The $(\text{NH}_4)_2\text{MoS}_4$ catalyst behaves as a bifunctional catalyst, showing both ring hydrogenation (more ethylbenzene (Figure 3d) and isopropyl benzene) and hydrogenolysis (more styrene (Figure 3c) and α -methylstyrene (Figure 3b)) activity. Carbon black does not produce a measurable effect at 370 C, but at temperatures above 400 C it has some ring hydrogenation activity as indicated by the higher yield of saturated products (ethylbenzene (Figure 3d) and isopropylbenzene).

Experiments on the thermal (non-catalytic) decomposition of Blind Canyon DECS-6 coal, waste rubber tire, commingled plastic, polyethylene and polystyrene samples were performed at a hydrogen pressure of 900 psi with a linear heating rate of 10 C/min. The weight loss profiles are shown in Figure 4. The TG curves indicate the different course of decomposition the various samples. Coal continues to lose weight due to pyrolysis and char gasification at temperatures up to 600 C. The high (33%) rubber residue must be mainly due to the presence of carbon black. The post-consumer plastic and polyethylene samples follow a similar weight loss course except for a slightly higher decomposition temperature and residue yield of the waste plastic. This is in agreement with the fact that polyethylene represents the main constituent of the commingled plastic. Polystyrene, on the other hand, decomposes at relatively low temperatures.

Co-processing runs of coal with waste rubber tire, commingled waste plastic, polyethylene and polystyrene (ratio 1:1) were carried out at a constant heating rate of 10 C/min under 900 psi hydrogen pressure. Figure 5 shows the TG curves of coal and polystyrene as an example of non-catalytic co-processing. The dotted line is the predicted weight loss curve of the mixture, which is the linear sum of their individual components. The mixtures of coal with the various polymers studied all show approximately additive rate and yield behavior when applying a 10 C/min heating rate. Because of the continuous temperature rise unimolecular decomposition reactions prevail and the total weight loss is primarily controlled by the thermal behavior of the individual components. However, when using a suitable isothermal procedure, as described previously for studying the catalytic effect, both the TG and GC/MS profiles indicate a strong interaction between the coal and the polystyrene (Figure 6). The weight loss of the mixture is increased compared to the predicted value at 370 C (Figure 6a). The results are confirmed by the total product evolution profiles. The coal has lost about 18% weight at the end of the 370 C period but volatile products are not detectable by MS due to their low intensity. Therefore, the total ion chromatogram is not shown in Figure 6. The yield of the volatile polystyrene products detectable at 370 C can be seen in the total ion chromatogram (TIC) in Figure 6b. Since the polystyrene is not yet completely degraded after 60 mins at 370 C, the remaining polystyrene reacts further when the temperature is increased, resulting in additional product evolution at temperatures above 400 C. The total ion chromatogram of the mixture (Figure 6c) shows that the products are formed mostly during the isothermal period. The strong interaction between coal and polystyrene may be due to some extent to the mineral matter in the coal acting as a catalyst and accelerating the decomposition of the polystyrene. Seehra et al. [11] studied mixtures of coal with polymers such as polystyrene, polyethylene and rubber tire by ESR techniques and reported that free radical concentrations are increased when mixing coal with polystyrene and polyethylene. This may well be due to the occurrence of interactions between

the feed components (or their intermediate products). The possible occurrence of these reactions can be another explanation for the increased weight loss of the mixture.

CONCLUSIONS

Isothermal runs at relatively low temperature (370 C) are found to be effective in bringing out differences between catalytic and thermal processes, whereas at linear heating rates of 10 C - 20 C/min thermal reactions overwhelm the catalytic effect.

The $\text{ZrO}_2/\text{SO}_4^{2-}$ superacid catalyst possesses high hydrogenolytic activity and causes a strongly increased rate of decomposition of SBR polymer at 370 C. The $(\text{NH}_4)_2\text{MoS}_4$ catalyst exhibits some ring hydrogenation activity at 370 C. Carbon black, on the other hand, has no measurable effect at 370 C, but shows some hydrogenation activity above 400 C.

Under thermally controlled (non-catalytic) conditions, mixtures of coal and polymers behave at first approximation in an additive manner. However, at lower temperatures, a synergistic effect is observed for polystyrene/coal mixtures.

High pressure TG/GC/MS is demonstrated to be a viable and useful technique for studying at a molecular level the effects of catalysts and blending under simulated process conditions, thus providing insight into the underlying reaction mechanisms.

ACKNOWLEDGEMENTS

The authors would like to thank Professor Larry L. Anderson and W. Tuntawiroon (University of Utah) for providing some of the samples. This work was sponsored by the Consortium for Fossil Fuel Liquefaction Science (DOE grant no. UKRF-4-23576-90-10).

REFERENCES

1. Liu, K., Jakab, E., McClennen, W.H., Meuzelaar, H.L.C., Prepr. Pap. Am. Chem. Soc., Div. Fuel Chem., 38 (1993), 823.
2. Huai, H., Tsai, C.H., Shabtai, J.S., Meuzelaar, H.L.C., Prepr. Pap. Am. Chem. Soc., Div. Fuel Chem., 37 (1992), 925.
3. Dworzanski, J.P., Chapman, J.N., Meuzelaar, H.L.C., Prepr. Pap. Am. Chem. Soc., Div. Fuel Chem., 37 (1992), 424.
4. Anderson, L.L., Tuntawiroon, W., Prepr. Pap. Am. Chem. Soc., Div. Fuel Chem., 38 (1993), 816.
5. Farcasiu, M., Chem Tech, January (1993), 22.
6. Taghiei, M.M., Huggins, F.E., Huffman, G.P., Prepr. Pap. Am. Chem. Soc., Div. Fuel Chem., 38 (1993), 810.
7. Farcasiu, M., Smith, C., J. Energy Fuels, 1991, 5, 83.
8. Derbyshire, F.J., Terrer, M.-T., Davis, A., Lin, R., Fuel, 1988, 67, 1029.
9. Zmierczak, W., Xiao, X., Shabtai, J., J. Energy Fuels 1994, in press.
10. Arata, K., Advances in Catalysis, 37, 1990, 165.
11. Ibrahim, M.M., Seehra, M.S., Prepr. Pap. Am. Chem. Soc., Div. Fuel Chem., 38 (1993), 841.

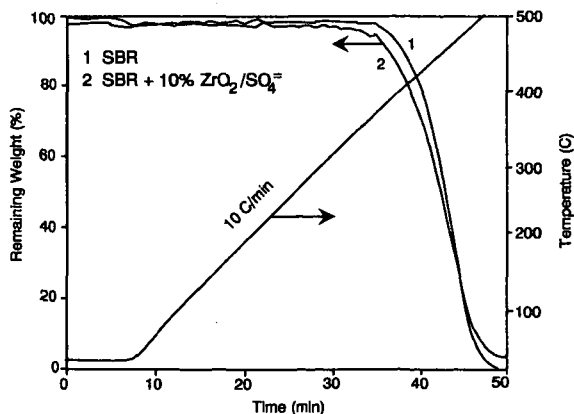


Figure 1. TG curves of SBR polymer at 900 psig (H_2).

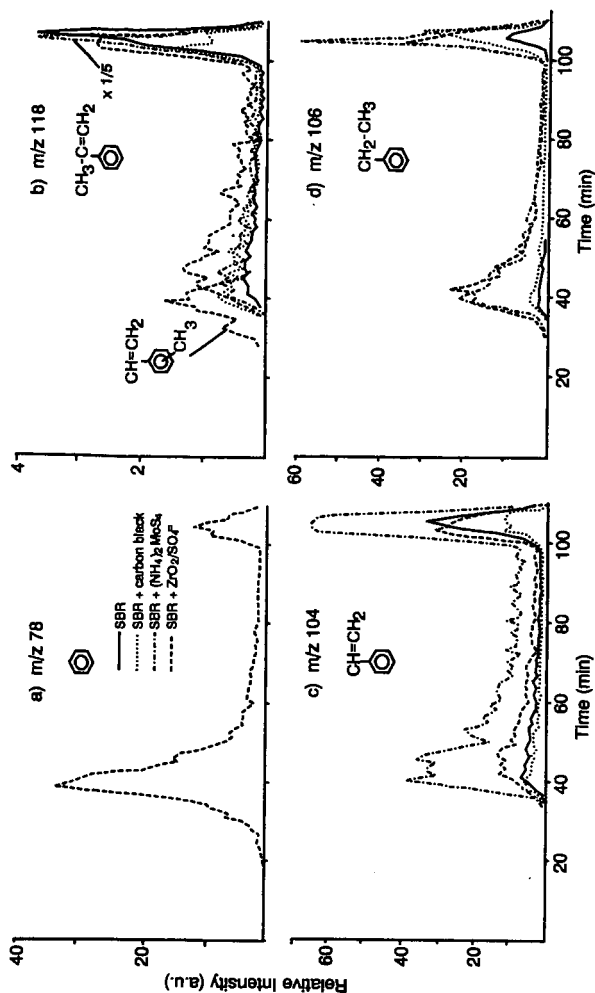


Figure 3. Effect of catalysts on evolution profiles of SBR polymer decomposition products. a) m/z 78, benzene; b) m/z 118, methylstyrene; c) m/z 104, styrene; and d) m/z 106 ethylbenzene.

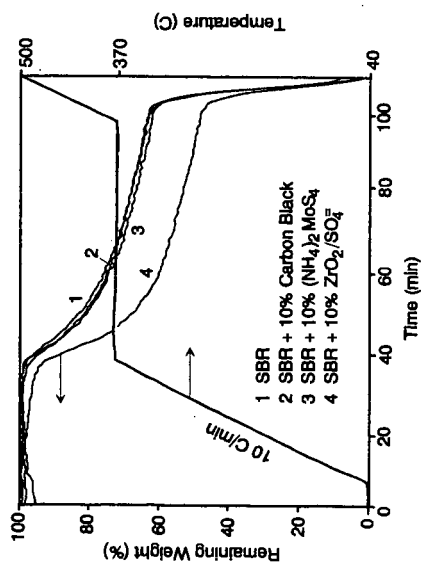


Figure 2. TG curves of SBR polymer with various catalysts at 900 psig (H_2).

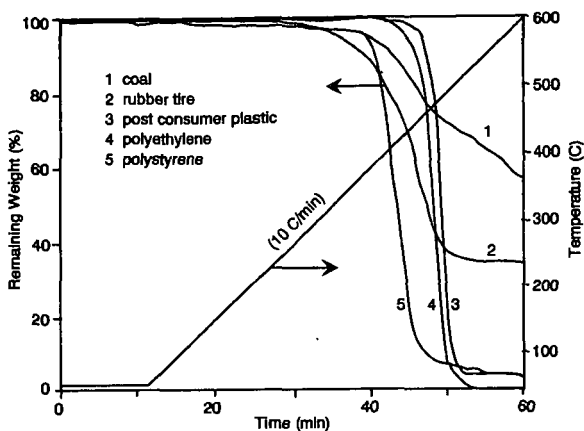


Figure 4. TG curves of various polymers at 900 psig (H_2).

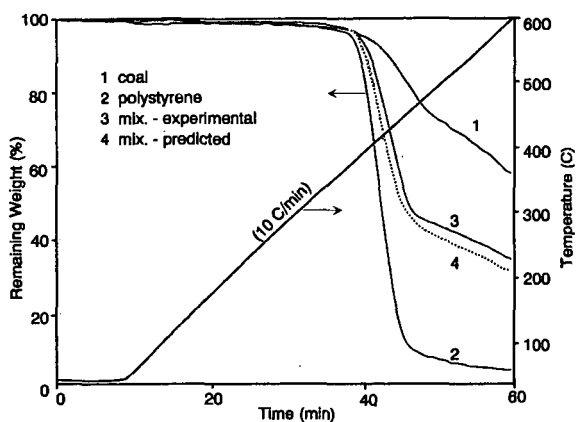


Figure 5. TG curves of coal and polystyrene at 900 psig (H_2).

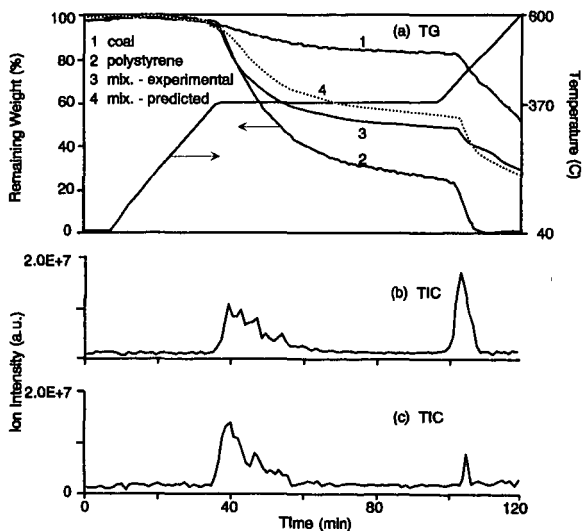


Figure 6. Effect of blending on coprocessing of coal and polystyrene at 900 psig (H_2). a) TG curves; b) total ion intensity profile of polystyrene; c) total ion intensity profile of coal and polystyrene.

THE USE OF THERMOGRAVIMETRIC ANALYSIS TO FOLLOW THE CONVERSION OF COAL DERIVED RESIDS IN THE RESID RECYCLING PROCESS

He Huang, W. H. Calkins* and M. T. Klein

Dept of Chemical Engineering, University of Delaware, Newark, DE 19716

Keywords: TGA, coal derived resid, resid conversion

INTRODUCTION

Direct Coal Liquefaction produces a substantial amount of high boiling non-distillable product (resid). The amount and character of this material depends upon the coal used and the conditions and reaction times in the liquefaction process. Because of its high boiling point and potential thermal instability, this material is not suitable for processing in a conventional petroleum refinery. In a commercial liquefaction process as it is visualized today, therefore, this material would be recycled to the process. Indeed, it has also been shown to actually have a beneficial effect in the liquefaction process(1).

Since these resids are complex and high boiling materials, their performance in the recycling process is not well understood or currently predictable. To this end, considerable analytical work has been accomplished for characterization purposes(2-5). These analyses have not really provided information about the reactivity of these resids under recycle conditions. Some measure of the ability to convert these resids to lower boiling, fuel-grade products is critically needed for design and scale up purposes. For example, it is important to know whether all resids are alike in their convertability, what conditions were optimum for their conversion, and what catalyst if any is needed for the conversion.

This has motivated the development of a coal-derived resid reactivity research program at the University of Delaware. A critical part of this program has been the development of a laboratory scale batch reactor(6) (Short Time Batch Reactor, STBR) capable of running liquefactions up to 450°C and 2500 psi at well defined reaction times from a few seconds to 30 minutes or longer. This reactor is simple in design and can be conveniently operated in the laboratory. In this STBR equipment, we have made a preliminary study of the actual conversion of coal liquefaction non-distillable resids to lower boiling, lower molecular weight material under conditions closely approximating the direct coal liquefaction process.

These resid conversion studies required a reasonably convenient means of determining the conversion of the resid from any particular experiment. For this purpose, we have relied heavily upon Thermogravimetric Analysis (TGA) augmented with Gas Chromatography and to a lesser extent GC/MS.

EXPERIMENTAL

Apparatus

The design and operation of the STBR reactor system were described at the 1993 national American Chemical Society meeting in Chicago (6).

The thermogravimetric analyzer (TGA) used is a Model 51 TGA (TA Instruments, New Castle Delaware). The gas chromatography was done on a Hewlett-Packard HP 5970 series II GC using a flame ionization detector. The gas chromatography/mass spectrometry was also performed on a Hewlett-Packard HP5970 series II using HP Series mass selective detector.

Materials Studied

The two coal derived 850 °F distillation resids were obtained from the Wilsonville Pilot Plant Runs 259 and 260, and prepared and composited by CONSOL Research. They are solids which were ground by CONSOL to about fourteen mesh. Ultimate analyses for these two resids are shown in Table 1.

The catalyst used was a presulfided Ni/Mo on alumina catalyst (Shell 324) (10.5 wt% Mo and 2.08 wt % Ni). The catalyst was presulfided in a distillate oil at the Wilsonville Plant. The oil was removed and the catalyst dried and ground under nitrogen by CONSOL.

Resid Conversion Reactions

All reactions were run as mixtures of tetralin (T, the donor solvent) and resid (R) over a range of T/R ratios and temperatures with and without catalyst.

Reaction Product Workup Procedure

The reaction product work up procedure is given in Figure 1. This resulted in the production of a liquid filtrate which consisted mainly of tetralin with dissolved resid and a solid filter cake which consisted of unconverted or partially converted resid. These two fractions were analyzed separately to determine the amount of resid that was converted.

TGA analysis on the liquid filtrate, which contained most of the tetralin, confirmed

that there was no mineral matter in the liquid sample (see Figure 2). This is critical, as our conversion measurements were based on comparison of the ash content of the converted product with that of the unreacted resid. As shown in Figure 2, the tetralin content of the liquid filtrate as well as the amount of higher boiling materials which were soluble in the liquid could be determined by TGA in nitrogen. The liquid filtrate was also analyzed by GC/MS and GC to determine the number of compounds dissolved in the tetralin from the resid conversion and to determine, if possible, their identities. However, much of the resid material which dissolved in the tetralin, even after the liquefaction reaction under the conditions used, was still too low in volatility to be detected with GC or GC/MS. The soluble material in the liquid consisted of some low boiling conversion products of the tetralin, some material in the original resid that was tetralin soluble, and also material formed by breakdown of the resid into tetralin soluble substances.

The tetralin soluble resid plus that solubilized in the liquefaction process was estimated by comparison of the ash content of the solid filter cake with that of the unreacted resid. The filtered solid resid was dried in a vacuum oven at 100 °C for 48 hr, then ground in a mortar and pestle and dried again to remove any residual tetralin. This is important, as change of the resid by the tetralin occurs during the TGA analysis itself (see Figure 3). A TGA run on the filtered solid resid is shown in Figure 4. TGA runs on the filtered solid resids give several characteristic parameters, such as VM (volatile matter), FC (fixed carbon), and Ash for an un-catalyzed sample(7). By running in nitrogen at a ramp of 10°C/min to 600 °C, the amount of volatile matter (VM) can be determined. Then, by introducing oxygen at 600°C, the loss in weight was observed. It is due to the oxidation of the combustible materials in the resid, so called "fixed carbon (FC)", leaving the residue as mineral matter or ash. Thereafter, it is run at a ramp of 100 °C/min to 900 °C in oxygen to determine any further oxidation of the ash residue at higher temperatures. As shown in Figure 4, there is no further loss in weight for un-catalyzed samples.

Determination of Catalyst Concentration

For a catalyzed sample, the 600 °C-oxidized residue includes the ash from the resid and partially oxidized catalyst. Since the mineral matter (ash) from the resid was used as a reference for determination of conversion, the amount of the residue must be corrected for the catalyst added. A TGA run on a solid resid with catalyzed sample is shown in Figure 5. For this catalyzed sample, VM determined by TGA consists of VM from resid and weight loss of the catalyst; FC determined by TGA represents FC from resid and the first stage of catalyst oxidation; Ash₁ determined by TGA contains ash from the resid and partially oxidized catalyst; and Ash₂ determined by TGA includes ash from the resid and ash from the catalyst. During the second oxidation period, i.e., the interval of the temperature ramped at 100 °C/min to 1000 °C in oxygen and kept at 1000 °C for 120 min, an additional loss in weight was obtained. It is due presumably to the oxidation of the sulfided catalyst to the oxides. This can be translated into catalyst concentration by comparison of the weight loss at 1000 °C with the weight losses obtained on catalyst alone and a calibration sample. A TGA run on the pure sulfided catalyst is demonstrated in Figure 6. Running in nitrogen at 10 °C/min to 600 °C, the first drop in weight loss was detected. As oxygen was added at 600 °C, the second drop in weight loss was obtained. This loss in weight is due to the partial oxidation of the catalyst, designated as the first stage of catalyst oxidation. When finally running in oxygen from 600 °C at 100 °C/min to 1000 °C and holding at 1000 °C for 120 min, the third drop in weight loss was observed. This loss in weight was due to the complete oxidation of the catalyst, designated as the second stage of catalyst oxidation, leaving the residue (so called "Ash₂") as the ash from the catalyst, i.e., metal oxides. As mentioned above, this third drop in weight loss is solely caused by the second stage of catalyst oxidation, because there is no such drop for the un-catalyzed resid sample alone (see Figure 4). Therefore, the amount of catalyst present in the resid-catalyst mixture is proportional to the third drop obtained by TGA, i.e.,

$$\text{Catalyst (wt\%)} = \alpha (\text{Ash}_1 (\text{wt\%}) - \text{Ash}_2 (\text{wt\%})) \quad (1)$$

where α is a scale constant which can be determined by a calibration sample, Ash₁ a 600 °C residue (wt%), and Ash₂ a 1000 °C residue (wt%). The amount of ash from the resid can be estimated by the mass balance of the ash in the resid and that from the catalyst. Since the ash from the catalyst (Ash_{catalyst}) and the ash from the resid (Ash_{resid}) are unchanged throughout the reactor runs, their ratio should be a constant, i.e.,

$$k = \frac{\text{Ash}_{\text{catalyst}} (\text{wt\%})}{\text{Ash}_{\text{resid}} (\text{wt\%})} \quad (2)$$

The constant k can be determined by running a calibration sample. For a catalyst-resid mixture, the final residue (Ash₂) by TGA includes ash from the resid and ash from the

catalyst. Therefore, we have another equation which can be used to solve simultaneously with Equation 2 for the amount of the ash from the resid:

$$Ash_{catalyst}(wt\%) + Ash_{resid}(wt\%) = Ash_2(wt\%). \quad (3)$$

Determination of Resid Conversion

Significant proportions of the resids are soluble in tetralin at room temperature (48 to 55 % for resid 1 and 37 to 42 % for resid 2, depending on the tetralin to resid ratio). During the liquefaction process, particularly in the presence of a catalyst, further solid resid becomes soluble in the tetralin. To the extent that this solubilization represents conversion of the resid, it can be estimated by comparing the amount of ash present in the solid filter cake (X) with that of the unreacted resid (X_0). The total amount of resid dissolved in the tetralin, D, can be calculated using the equation:

$$D(wt\%) = (1 - \frac{X_0}{X}) \times 100(wt\%). \quad (4)$$

D of course is the sum of the soluble resid and the resid which has become solubilized in the conversion process. Conversion can be estimated by subtracting the soluble portion of the resid D at time zero, from the D at time t. Equation 4 is valid because no inorganic matter (ash) goes into the liquid (see Figure 2). When catalyst is used, the ash determined by TGA must be corrected for the ash from the catalyst added.

RESULTS AND DISCUSSION

The experimental error for determination of the TGA characteristic variables (VM, FC, and Ash) is less than $\pm 0.5\%$ of the measured values. A TGA run on a liquid filtrate shown in Figure 2 gives two fractions: a fraction boiling in the tetralin range and a higher-boiling tetralin soluble fraction. TGA measurements can not discriminate among the converted components whose boiling points are close to tetralin. Therefore, GC and GC/MS were used to detect them. Tests on both un-catalyzed and catalyzed samples by GC and GC/MS have shown that there is some (up to 0.5 wt% for un-catalyzed runs, and 2 wt% for catalyzed runs) of material in the liquid filtrate boiling close to tetralin, which is formed by breakdown of resid. This represents about 5% to 20% conversion of the resid which has been converted to low boiling material. These low boiling substances consist of more than 50 individual compounds detected by GC, each too low in concentration to be identified. The GC/MS used in this work is not sensitive enough to detect these many low boiling materials in the very low concentrations involved.

The percent resid dissolved in tetralin (D) was calculated using Equation 4. A portion of the resid is tetralin soluble even at room temperature. To visualize the source of the dissolution portion in the resids under various conditions, resid-normalized VM, FC and D are plotted with various conditions for Resid 1 in Figure 7. It is obvious that the majority of the dissolution portion (about 80 wt%) comes from the VM in the resid.

For un-catalyzed 30 min reactor runs of Resid 1, the percent resid dissolved in tetralin (D) increases only about 1 wt% at 412 °C, and only about 6 wt% at 435 °C for T/R = 3.0 samples. For un-catalyzed 30 min reactor runs of Resid 2, the percent resid dissolved in tetralin (D) increases about 2 wt% at 410 °C, and about 13 wt% at 434 °C for T/R = 3.0 samples, which shows about twice the reactivity as resid 1.

Evolution rate versus temperature (DTG vs. T curve) of these uncatalyzed liquid samples were determined on the liquid filtrate from the calibration sample (treated with tetralin at room temperature), and resid 1 reacted for 5 min at 434 °C, and for 30 min at 435 °C. The results as plotted in Figure 8 indicate a bimodal distribution in the evolution pattern. There is no observable change in the evolution pattern through the reactor runs under the experimental conditions we have used in this project, although the material went into solution. A similar evolution rate vs. temperature of the liquid samples for the resid 2 conversion at 435 °C is obtained. There is also no significant change in the molecular weight distribution (evolution temperature pattern) in the liquid filtrate.

Plots of the D vs. reaction times for resid 1 at different temperatures and at T:R:Cat. (Tetralin:Resid:Catalyst) = 3:1:1 are shown in Figure 9. For reaction temperature around 415 °C, the percent resid dissolved in tetralin (D) increases with reaction time up to about 10% for 30 min (ten times higher than the un-catalyzed run). For a reaction temperature around 434 °C, the percent resid dissolved in tetralin (D) increases with reaction time up to 20 min, then it levels off. In 20 min, it increases to about 17% (four times higher than un-catalyzed runs). Plots of the D vs. reaction times for resid 2 at different temperatures and at T:R:Cat. = 3:1:1 are similar to the plots in Figure 9. For a reaction temperature around 415 °C, the percent resid dissolved in tetralin (D) increases with reaction time up to about 31.6% for 30 min (fifteen times higher than un-catalyzed runs). For a reaction temperature around 440 °C, it increases with reaction time up to 10 min, then it levels off. In 10 min, it

increases to about 33.2% (eight times higher than un-catalyzed runs). It is interesting to point out that:

1. in the lower temperature runs, they approached the same value of D in high temperature runs at longer reaction time (Figure 9);
2. at reaction time 30 min, the percent resid dissolved in tetralin (D) on an ash-free basis for 421 °C approaches about 87% and that for 442 °C to about 91%;
3. the reactivity of the resid 2 in catalyzed conversion is higher than that of the resid 1, the similar order which is observed in un-catalyzed conversion.

To examine the evolution pattern (a function of the molecular weight distribution) of the converted materials in the liquid filtrate, slow ramp TGA (1 °C/min) was run on selected liquid samples. Evolution rate vs. temperature of the liquid samples from the catalyzed resid 1 conversion: 0 min (the liquid filtrate from calibration sample, which is treated with tetralin at room temperature), 5 min at 434 °C, and 30 min at 435 °C for resid 1 was plotted in Figure 10. This shows that the evolution rate for reactor runs significantly shifted to lower temperature. In other words, there is a notable reduction in the average molecular weight by the catalyst. This can be quantitatively described by two characteristic variables: peak evolution temperature (T_{peak}) and mean evolution temperature (T_{mean}). T_{peak} is defined as the evolution temperature at maximum evolution rate. T_{mean} is defined as the mean evolution temperature weighted by the evolution rate. Mathematically,

$$T_{mean} = \frac{\sum_i (Evolution Rate)_i T_i}{\sum_i (Evolution Rate)_i} \quad (5)$$

The calculated T_{peak} and T_{mean} for the catalyzed runs and reference sample (at 0 min) are listed in Table 2. For longer reaction time, not only T_{mean} decreases by about 60 °C, but also T_{peak} shifted to lower temperature direction by about 50 °C. The same behavior was observed in the resid 2 catalyzed conversion. It is interesting to note from Figures 8 and 10 that the soluble fraction of the resids shows a bimodal distribution of differential evolution peaks in the TGA. The higher temperature peak disappears after catalytic reactions, but is unchanged in reactions without catalyst.

SUMMARY AND CONCLUSIONS

1. The combination of reaction in the STBR (Short Time Batch Reactor) with TGA analysis of the liquid filtrates and the "un-converted" filtered solid resids provides a direct and reproducible means of indicating the breakdown of coal-derived liquefaction resids under liquefaction conditions.
2. The conversion of resid to tetralin soluble material is determined by relating the inorganic matter (ash) in the reacted resid with that of the un-reacted resid. Conversion of un-catalyzed tetralin-insoluble resids to tetralin soluble products in this study was very low (< 10 wt%) under coal liquefaction conditions, however, up to 50 wt% of the resid is tetralin-soluble at room temperature.
3. Up to 80% (ash-free basis) of the room temperature tetralin insoluble resid is solubilized in tetralin using sulfided Ni/Mo on alumina catalyst at 434 °C for 10 min.
4. A method has been devised for determining the catalyst concentration and the ash from the resid by TGA.
5. The two resids examined showed somewhat different reactivities.
6. In the catalyzed experiments, a progressive decrease in the temperature evolution range (as measured by TGA) of the solubilized materials with time under liquefaction conditions is observed by TGA. In the un-catalyzed experiments, no change in the evolution range of the solubilized materials with time up to 30 min is observed by TGA.
7. The majority of tetralin soluble or solubilized materials come from the volatile matter in the resids.
8. While liquefaction conditions, particularly in the presence of Ni/Mo on alumina catalyst are effective in converting tetralin insoluble to tetralin soluble material and in reducing the average molecular weight (as shown by TGA), only a small fraction (perhaps 20 percent) of this material is converted to the boiling range of gasoline or diesel fuel under the liquefactions conditions studied (30 minutes at 434 °C) as shown by GC.

ACKNOWLEDGEMENTS

The Assistance and advice of F.P. Burke, R.A. Winschel and S.D. Brandes of CONSOL Inc in preparation and analysis of the resid and catalyst samples used in this project is gratefully acknowledged. This work was supported by subcontract from CONSOL Inc. under U. S. DOE Contract No. DE-AC22-89PC89883.

REFERENCES

- 1 Whitehurst, D.D., Mitchell, T.O., and Farcasiu, M. *Coal Liquefaction* Academic Press, Chapter 7, p.192 (1980)
- 2 Ibrahim, M.M. and Seehra, M.S. *DOE/PC 89883-57* Oct 1992
- 3 Malhotra, R. and McMillan, D. *DOE/PC 89883-39* Jan 1992
- 4 Solum, M.S. and Pugmire, R.J. *DOE/PC 89883-65* Nov. 1992
- 5 Stock, L.M. and Cheng, C. *DOE/PC 89883-64* Nov 1992
- 6 Huang, H.; Calkins, W.H.; and Klein, M.T. *ACS Fuel Division Preprints* 38 (3), 1080 (1993)
- 7 Ottaway, M. *Fuel*, 61 (8), 713 (1982)

Table 1 Ultimate Analyses of the Two Resids

| Sample | Ultimate (wt% MAF): | | |
|-------------------------------------------------------|---------------------|--|-------|
| Resid 1 | C | | 90.24 |
| Plant: Wilsonville | H | | 6.39 |
| Run Number: 259 | N | | 1.05 |
| Sample Designator: V1067 | S | | 1.49 |
| Sampling Point: 2nd Stage Product | O (dif) | | 0.83 |
| Feed Coal: Pittsburgh Seam, Ireland Mine | Ash, wt% as det. | | 10.21 |
| Resid 2 | C | | 91.03 |
| Plant: Wilsonville | H | | 6.56 |
| Run Number: 260 | N | | 1.15 |
| Sample Designator: V1067 | S | | 0.09 |
| Sampling Point: 2nd Stage Product | O (dif) | | 1.17 |
| Feed Coal: Wyodak & Anderson Seam, Black Thunder Mine | Ash, wt% as det. | | 18.30 |

Table 2 Peak Evolution Temperatures (T_{peak}) and Mean Evolution Temperatures (T_{mean}) of the Liquid Filtrates from the Catalyzed Resid Conversion

| Sample | T_{peak} , °C | T_{mean} , °C |
|---------------------------|-----------------|-----------------|
| <u>Resid 1 + Catalyst</u> | | |
| 0 min | 320 | 349 |
| 5 min at 434 °C | 318 | 322 |
| 30 min at 435 °C | 273 | 291 |
| <u>Resid 2 + Catalyst</u> | | |
| 0 min | 307 | 321 |
| 30 min at 442 °C | 274 | 282 |

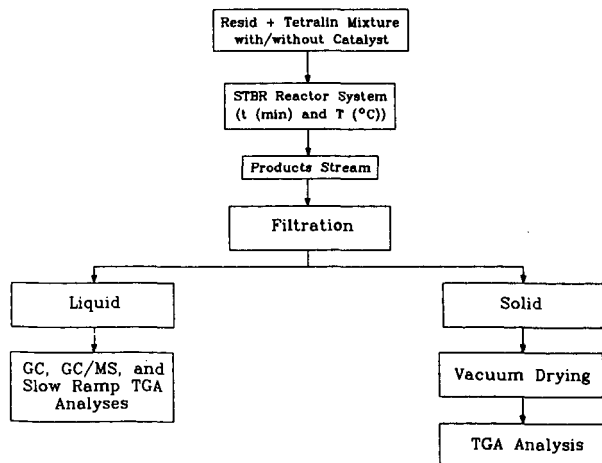


Figure 1 Schematic Diagram of the Experimental Procedure

Sample: CC2006, Liquid Filtrate
 Size: 44.3420 mg
 Method: Resid Conversion II
 Comment: Reactor Run CC2006, Catalyzed Resid 2 Conversion, 30 min, 442 °C

TGA

File: C: CC2006L.01
 Operator: Dr. Huang, He
 Run Date: 4-Oct-93 07:06

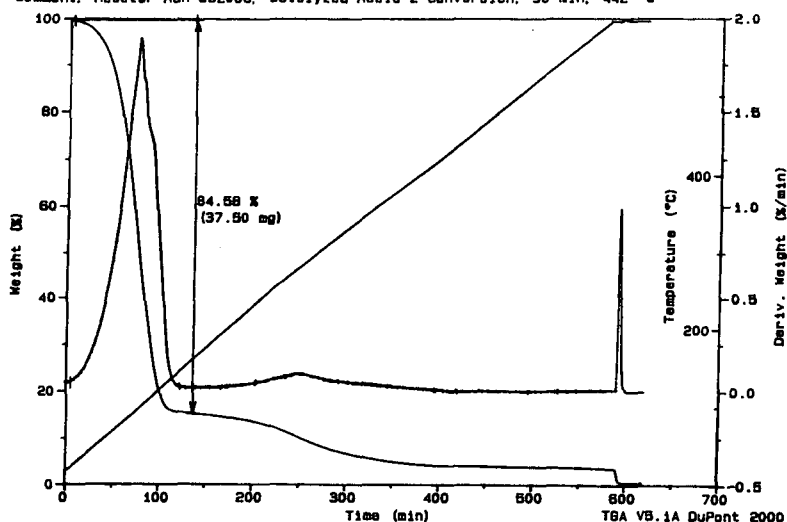


Figure 2 A TGA Run on a Liquid Filtrate of Catalyzed Reactor Run

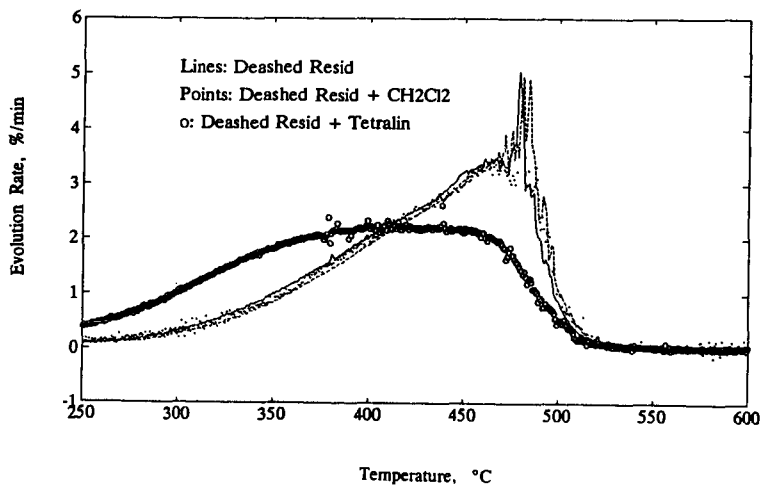


Figure 3 Effect of tetralin on TGA Analysis

Sample: C2024, Filtered Solid Resid
 Size: 41.0520 mg
 Method: Resid Conversion
 Comment: Reactor Run C2024, Resid 2 Conversion, 30 min, 434 °C

TGA

File: C:\C2024S.001
 Operator: Dr. Huang, He
 Run Date: 8-Sep-93 12:52

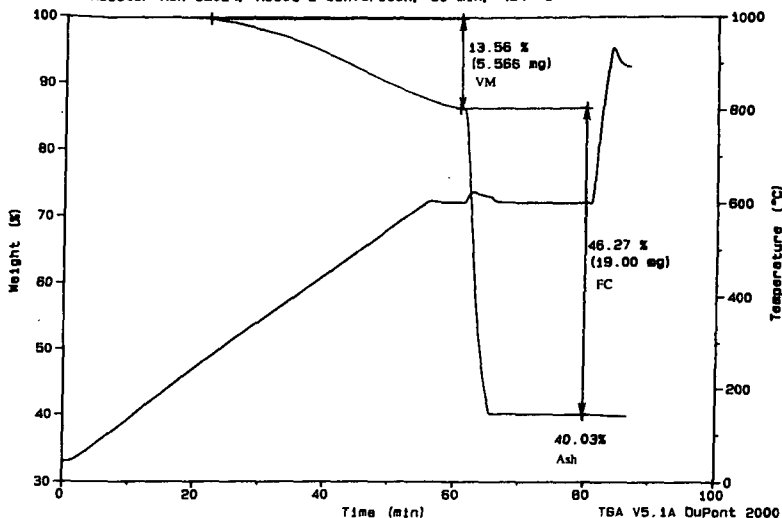


Figure 4 A TGA Run on a Filtered Solid Resid of Un-catalyzed Reactor Run

Sample: CC2004, Filtered Solid Resid
 Size: 49.1590 mg
 Method: Resid Conversion - Cat
 Comment: Reactor Run CC2004, Catalyzed Resid 2, 10 min, 436 °C

TGA

File: C:\CC2004S.001
 Operator: Dr. Huang, He
 Run Date: 20-Sep-93 09:14

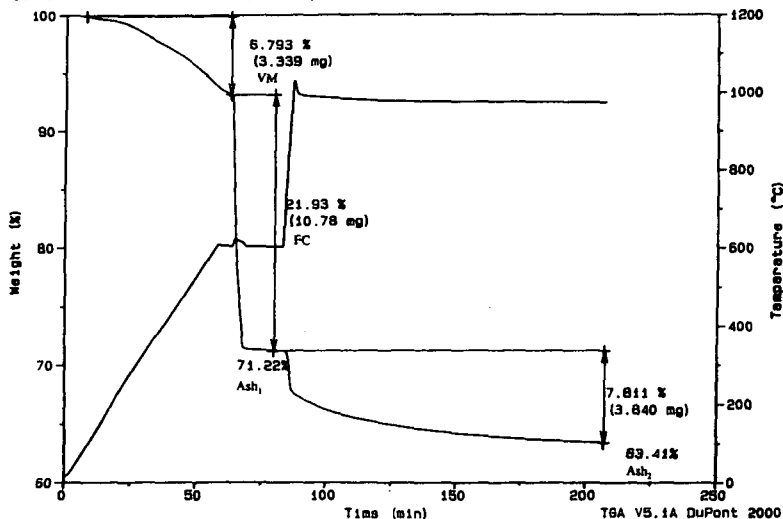


Figure 5 A TGA Run on a Filtered Solid Resid of Catalyzed Reactor Run

Sample: Pure Sulfided Catalyst
 Size: 38.7200 mg
 Method: Resid Conversion
 Comment: Catalyst: Sulfided Mo-Ni on Alumina (Shell 324)

TGA

File: C: CAT.002
 Operator: Dr. Huang, Ho
 Run Date: 13-Aug-93 18:37

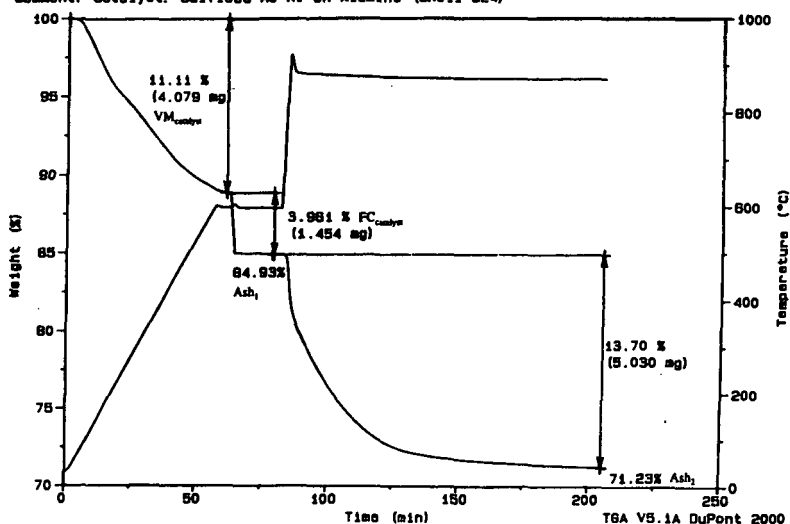


Figure 6 TGA Curves of the Pure Sulfided Catalyst of Mo-Ni on Alumina

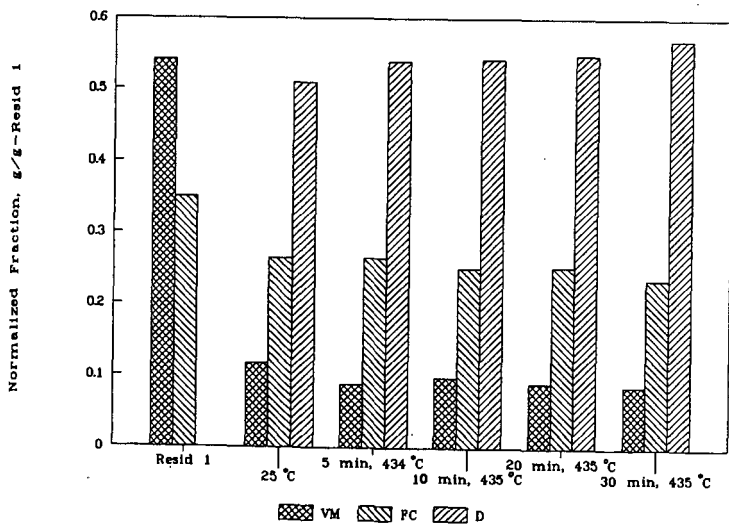


Figure 7 Resid-normalized VM, FC and D in the Resid 1 Treated or Reacted with Tetralin under Various Conditions (T/R = 3.0)

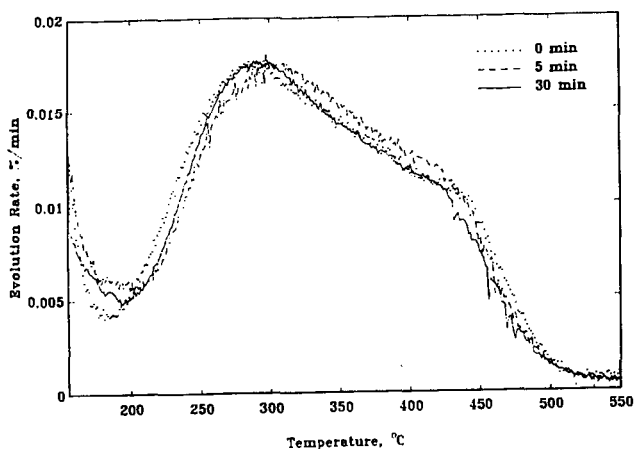


Figure 8 Evolution Rate (DTG) Versus Temperature Determined by Slow Ramp TGA (5 °C/min) for the Liquid Filtrates of Un-catalyzed Resid 1 Conversion (T/R = 3.0): 0 min, 5 min at 434 °C, and 30 min at 435 °C

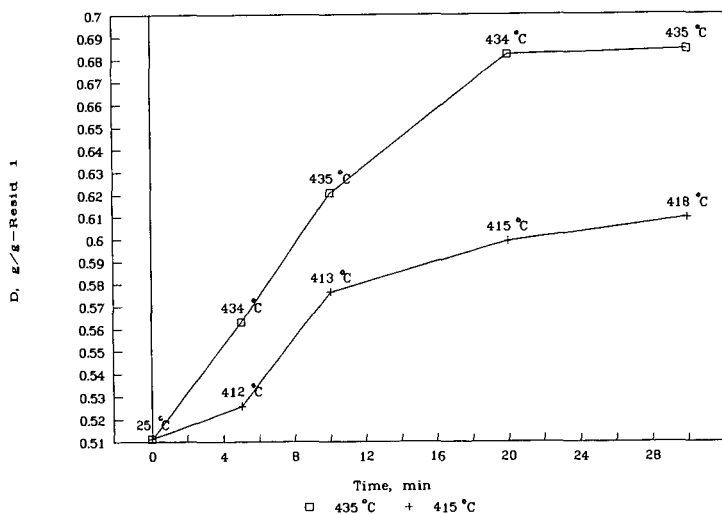


Figure 9 Percent Resid Dissolved in Tetralin (D) Versus Reaction Time of Catalyzed Resid 1 Conversion at Two Temperatures (T/R:Catalyst = 3:1:1)

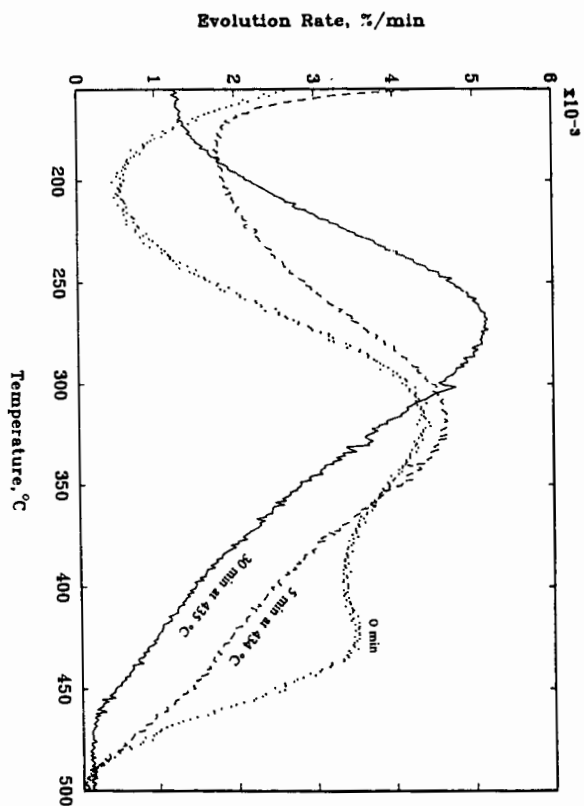


Figure 10 Evolution Rate (DTG) Versus Temperature Determined by Slow Ramp TGA ($1^{\circ}\text{C}/\text{min}$) for the Liquid Filtrates of Catalyzed Resid 1 Conversion (T/R = 3.0): 0 min, 5 min at 434 $^{\circ}\text{C}$, and 30 min at 435 $^{\circ}\text{C}$